SPE 131350

From Oil-Prone Source Rock to Gas-Producing Shale Reservoir – Geologic and Petrophysical Characterization of Unconventional Shale-Gas Reservoirs

Q. R. Passey, K. M. Bohacs, W. L. Esch, R. Klimentidis, and S. Sinha, ExxonMobil Upstream Research Co.

This paper was prepared for presentation at the CPS/SPE International Oil & Gas Conference and Exhibition in China held in Beijing, China, 8–10 June 2010.

Abstract

Many currently producing shale-gas reservoirs are overmature oil-prone source rocks. Through burial and heating these reservoirs evolve from organic-matter-rich mud deposited in marine, lacustrine, or swamp environments. Key characterization parameters are: total organic carbon (TOC), maturity level (vitrinite reflectance), mineralogy, thickness, and organic matter type. Hydrogen-to-carbon (HI) and oxygen-to-carbon (OI) ratios are used to classify organic matter that ranges from oil-prone algal and herbaceous to gas-prone woody/coaly material.

Although organic-matter-rich intervals can be hundreds of meters thick, vertical variability in TOC is high (<1-3 meters) and is controlled by stratigraphic and biotic factors. In general, the fundamental geologic building block of shale-gas reservoirs is the parasequence, and commonly 10's to 100's of parasequences comprise the organic-rich formation whose lateral continuity can be estimated using techniques and models developed for source rocks.

Typical analysis techniques for shale-gas reservoir rocks include: TOC, X-ray diffraction, adsorbed/canister gas, vitrinite reflectance, detailed core and thin-section descriptions, porosity, permeability, fluid saturation, and optical and electron microscopy. These sample-based results are combined with full well-log suites, including high resolution density and resistivity logs and borehole images, to fully characterize these formations. Porosity, fluid saturation, and permeability derived from core can be tied to log response; however, several studies have shown that the results obtained from different core analysis laboratories can vary significantly, reflecting differences in analytical technique, differences in definitions of fundamental rock and fluid properties, or the millimeter-scale variability common in mudstones that make it problematic to select multiple samples with identical attributes.

Porosity determination in shale-gas mudstones is complicated by very small pore sizes and, thus, large surface area (and associated surface water); moreover, smectitic clays that are commonly present in mud have interlayer water, but this clay family tends to be minimized in high maturity formations due to illitization. Finally, SEM images of ion-beam-milled samples reveal a separate nano-porosity system contained within the organic matter, possibly comprising >50% of the total porosity, and these pores may be hydrocarbon wet, at least during most of the thermal maturation process. A full understanding of the relation of porosity and gas content will result in development of optimized processes for hydrocarbon recovery in shale-gas reservoirs.

Introduction/Background

The term "unconventional reservoirs" covers a wide range of hydrocarbon-bearing formations and reservoir types that generally do not produce economic rates of hydrocarbons without stimulation. Common terms for such "unconventional" reservoirs include: Tight-Gas Sandstones, Gas Hydrates, Oil Shale formations, Heavy Oil Sandstones, and Shale Gas, among others. The focus of this paper is to discuss the geological genesis and characterization of the class of "unconventional" reservoirs commonly termed Shale Gas.

Shale is a term that has been applied to describe a wide variety of rocks that are composed of extremely fine-grained particles, typically less than 4 microns in diameter, but may contain variable amounts of silt-size particles (up to 62.5 microns). In

comparison, sandstones are rocks composed of grains (of variable composition) that are typically between 62.5 microns and 2000 microns in diameter. Just as sandstones can be composed of different mineral grains (e.g., quartz, feldspar, rock fragments, clays, etc.), shales (more properly referred to as mudstones) also exhibit a wide range in composition (clay, quartz, feldspar, heavy minerals, etc.). Moreover, the composition of a "typical" mudstone will vary much more than for typical sandstones, even though to the naked eye, many mudstones (i.e., shales) look similar.

Depositional and Geologic Controls on Organic Richness

Recent studies indicate that although these organic-matter-rich mudstone formations may be hundreds of meters in gross thickness (and may appear largely homogeneous), the vertical variability in the organic richness can vary on relatively short vertical scales (often much less than 1 meter; e.g., Bohacs, 1998; Bohacs et al., 2005; Guthrie and Bohacs, 2009). The vertical heterogeneity observed can be directly tied back to geologic and biotic conditions when deposited; keep in mind that these fine-grain sediments are deposited very slowly and with subsequent compaction and lithification, a 1 meter thick interval of rock may represent thousands to millions of years of time. In essentially all organic-rich mudstones, the basic building blocks conform to well-understood stratigraphic controls and architectures. The basic unit can been described as a parasequence (an upward shoaling package of genetically related beds and bedsets) or its equivalent. This depositional pattern is commonly repeated dozens of times, stacked into parasequence sets and ultimately bounded by sequence boundaries. The rigorous characterization of these packages allows for the understanding and exploration of the best intervals.

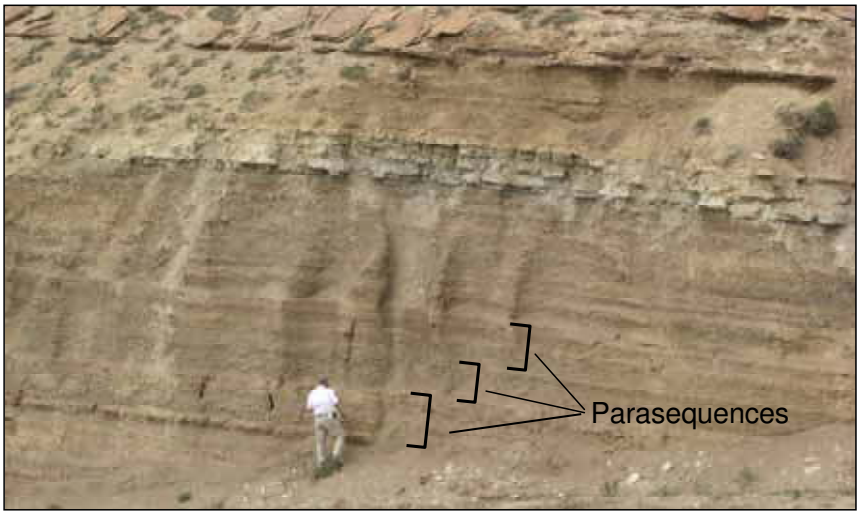

Figure 1 - Outcrop of Green River Shale, Luman Tongue, Hiawatha Section. Green River Basin, Wyoming, USA. illustrating the occurrence of 1-2 meter thick parasequences, which are the primary building blocks of organic-matter-rich packages.

The accumulation of organic-matter-rich rocks (ORRs) is a complex function of many interacting processes (as discussed more fully in Bohacs et al., 2005). Successful prediction requires the integration of plate tectonics, geodynamics, and basin structural development with reconstructions of paleo-environmental conditions as the context for process-based models for the occurrence, distribution, and character of potential source rocks or shale-gas reservoirs. Organic-matter accumulation in depositional environments is controlled by complex, non-linear interactions of three main proximate control variables: rates of production, destruction, and dilution. Significant enrichment of organic matter occurs where organic-matter production is maximized, destruction is minimized, and dilution by clastic or biogenic material is optimized, in an area with sufficient accommodation rates to accumulate significant thickness of sediments. The main factors and interactions are illustrated in the following paragraphs.

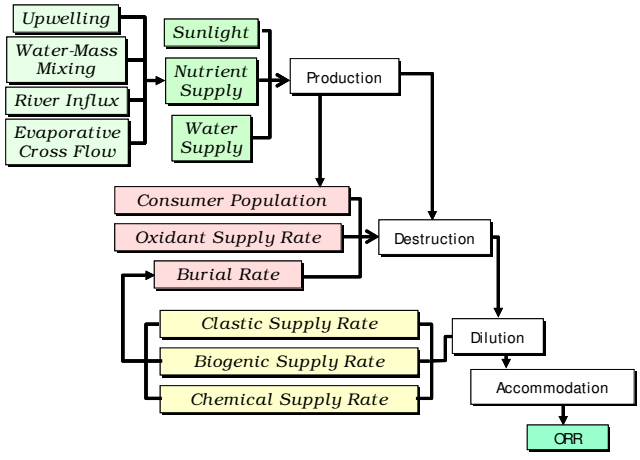

Figure 2 - Controls on organic-richness highlighting the interconnected nature of the processes of organic production, destruction, and dilution and the factors that influence them.

Production: Organic production provides the raw material upon which an ecosystem acts. Its primary proximate controls are the supply rates of solar energy, nutrients, and water. Equations 1a, and 1b indicate the relations among nutrient input and population growth of various organism classes: primary producers that generate organic-carbon rich material, and secondary consumers such as radiolaria that provide brittle material (e.g., silica). As the equations illustrate, population growth rates are quite different among these two classes of organisms because of their reproductive strategies and limits of ecosystem capacity. Both are, however, ultimately influenced by nutrient supply and solar energy input through both *r,* the inherent growth rate of the organism and *K*, the carrying capacity of the ecosystem. The equations also indicate some of the interconnections among production, destruction, and dilution illustrated in Figure 2-- nutrients are supplied to an ecosystem by the same water circulation processes that can carry destruction-enhancing oxidants, dilution-enhancing clastics, and suspended sediment that can block sunlight, decreasing production.

Production is, therefore, seldom sufficient by itself to generate significant organic accumulations because both very low and very high rates of production are detrimental to accumulations of ORR: very low rates cannot keep up with rates of destruction by consumer organisms and very high rates lead to significant dilution by non-hydrogen-rich biogenic material (tests, shells, bones; e.g., Monterey Formation and Mowry Formation examples in Bohacs et al., 2005— see also discussion in Tyson 1995). This effect is particularly significant in strata younger than Early Jurassic because of the evolutionary radiation of coccolithophores (calcareous primary producers) and is exacerbated in high-production regimes since the Late Cretaceous with the emerging dominance of diatoms (siliceous primary producers -- e.g., Berger 1976; Bogdanov et al. 1980a; Tada 1991). Organic accumulation in the rock record appears to be optimized at intermediate rates of primary organic production (e.g., Strakhov 1971; Brumsack 1980; Summerhayes and Masran 1983; Isaacs 1987; Bogdanov et al. 1980b; Schwalbach et al. 1993; Tyson 1995, 2001).

EQUATION 1a: Production rate relation for primary producers of organic carbon ('r-controlled', generalist organisms). Key factors are previous population size (N_o, a function of nutrient supply history) and inherent organism growth rate (r).

$$\frac{\partial P}{\partial t} = N_o e^{-rt}$$

EQUATION 1b: Production rate relation for secondary consumers that can supply such brittle biogenic material as silica ('K-controlled', specialist organisms). Key factors are also previous population size (N_o, a function of nutrient supply history-- mostly the primary producers governed by Equation 1a) and inherent organism growth rate (r), as well as the carrying capacity of the ecosystem (K), itself a function of nutrient supply and oxygen supply (see Equation 2a), among other factors.

$$\frac{\partial P}{\partial t} = \frac{KN_o}{\left(K - N_o\right)e^{-rt} + N_o}$$

Destruction: Organic-matter destruction occurs through ingestion by metazoans, microbial respiration, and inorganic oxidation (Equations 2a and 2b). Most organic matter is consumed within the photic zone; typically less than 10% escapes these upper 50 to 100 meters of the water column. Most of the organic matter that reaches the sea floor is consumed by metazoans and microbes in the upper decimeters of the sediment column. Destruction processes are distinctly threshold governed—for example, metazoan organisms are excluded only below certain oxygen concentrations (e.g., Savrda and Bottjer 1986, 1991). As Equation 2a indicates there are numerous oxidant species that can degrade organic matter (oxygen, sulfate, nitrate, iron, etc.).

The key factor for preservation of organic matter is maintenance of low oxidant concentrations in the sediment pore-water system, through restricted advection of oxidants in the water column and diffusion through shallow sediments. Burial rates must also be sufficiently fast to limit oxidant exposure times and move organic matter out of the shallow zone below the sea floor of most active degradation and oxidant resupply relatively quickly (e.g., Hartnett et al. 1998). As Figure 2 illustrates, the optimal burial rate includes the accumulation of both inorganic and organic material, so estimates of organic-matter destruction must factor in both primary production of hydrogen-poor biogenic material (along the lines of Equation 1b) and dilution by hydrogen-poor clastic material (see Equation 3a).

EQUATION 2a: Oxidation and respiration component of destruction rate: Oxidant level is a function of the relative magnitude of advected and diffused oxidant supply rates versus oxidant utilization by organic matter degradation:

$$\frac{\partial O}{\partial t} = \underbrace{u\frac{\partial O}{\partial x} + v\frac{\partial O}{\partial y} + w\frac{\partial O}{\partial z}} + \underbrace{\sum_{i=1}^{n} O_i \frac{\partial \eta}{\partial t} + O_i \frac{\partial \eta}{\partial z}} - \underline{\widehat{O}}$$

= advection of oxidants + diffusion of oxidants – local oxidant consumption

EQUATION 2b: Functional form of secondary consumer component of destruction rate for specific pairs of consumer and producer organisms-- population growth rate of secondary consumers is a function of the growth rate of primary producers, previous population size, and carrying capacity of the ecosystem:

$$\frac{\partial P}{\partial t} = \left[\frac{KN_o}{(K - N_o)e^{-rt} + N_o} \right] - \left[N_o e^{-rt} \right]$$

= secondary consumer growth – primary producer growth

Dilution: Organic-matter-rich rocks require a critical concentration of organic matter to function as effective hydrocarbon sources or shale-gas reservoirs. Dilution of organic matter by material that is not hydrogen rich is the predominant control on significant accumulations of organic matter because it has the widest range of mass-accumulation rates and grain size variations (Bohacs et al., 2005). Dilution can be by either clastic or biogenic material or both (Equations 1a, 1b, 3a, and 3b). Equation 3a indicates that clastic dilution (in terms of sediment flux rates) is non-linear and threshold governed -- most sensitive to shear stress ($\propto$ flow velocity and depth) above the critical value for initiating and maintaining sediment motion. Hence, it is apparent that flow velocities are a key factor in the accumulation of organic matter -- it very strongly controls dilution, as well as affecting the advection of nutrients, suspensates, and oxidants for production and destruction. The threshold velocity for sediment movement is a function of grain size and its density relative to that of the transporting medium. This relation is reasonably accurate for cohesionless grains under traction transport, but each of these attributes vary significantly in mud-dominated systems— although much mud is transported as aggregates or floccules, their size and density range widely and change during transport (e.g., Schieber et al., 2007). Significant volumes of mud are also carried in suspension that changes the density of the transporting fluid and follow a different transport relation ($\propto$ suspended sediment concentration and bottom slope; e.g., van Rijn, 1984). A significant factor in the formation and stability of mud aggregates is the presence and concentration of organic matter, especially extra-cellular polysaccharides that are effective binding agents (Passow et al., 1994; Logan et al., 1995). Consuming organisms also ingest and 'package' mud-sized material into sand-sized pellets (e.g., Grossart et al., 1997). Thus organic-matter production and destruction rates influence the partitioning and interchange between bed-load and suspended load transport of diluting mud as well as the size and persistence of mud aggregates/floccules ($\propto$ transport rate).

Production of biogenic non-hydrogen-rich material can also be a significant factor in dilution. High biogenic dilution rates can produce relatively organic-lean, but brittle rocks in distal, low-advection environments (*e.g.*, Monterey Formation, Mowry Shale). Low dilution rates are a necessary, but seldom sufficient condition for organic accumulation. There is an optimal rate of sediment accumulation that maximizes the portion of organic carbon that is preserved through early degradation during shallow burial (or the "burial efficiency" of Heinrichs and Reeburgh 1987). In Equation 2a, it is the accumulation of a sufficient thickness of relatively impermeable mud that limits diffusion of oxidants from the overlying water mass ($O_i\, \partial\eta/\partial z$).

EQUATION 3a: Sediment transport relation indicating the functional form of cohesionless siliciclastic dilution processes (after Wong and Parker, 2006):

$$q_s = \left(D\sqrt{\left(\frac{\rho_s - \rho}{\rho} \right) gD} \right) * \left[4\left(\frac{\tau - \tau_c}{(\rho_s - \rho)gD} \right)^{3/2} \right]$$

= resistance of particle to motion * fluid shear stress in excess of threshold of motion

EQUATION 3b: Population net growth relation indicating functional form of biogenic dilution processes:

$$\frac{\partial P}{\partial t} = \mu(N, I) - mP - \nu \frac{\partial P}{\partial z} + \kappa \frac{\partial^2 P}{\partial z^2}$$

= phytoplankton growth rate - consumption - sinking + mixing

When or where clastic input is the primary control on organic-matter content, the vertical distribution of TOC can be indicative of either individual parasequences, or of parasequence sets reflecting an overall progradation or transgression within a sequence. In these settings (commonly relatively proximal to shoreline), the vertical profile of TOC, either measured on closely spaced samples or estimated from well logs, provides an excellent proxy for identification of parasequences (or parasequence sets) as illustrated in Figure 3. In this situation, the characteristic "high TOC at the base, decreasing upward" signature of parasequences is readily identified (Creaney and Passey, 1993) and is useful for stratigraphic correlation as part of estimating resource distribution, as

discussed in the following section.

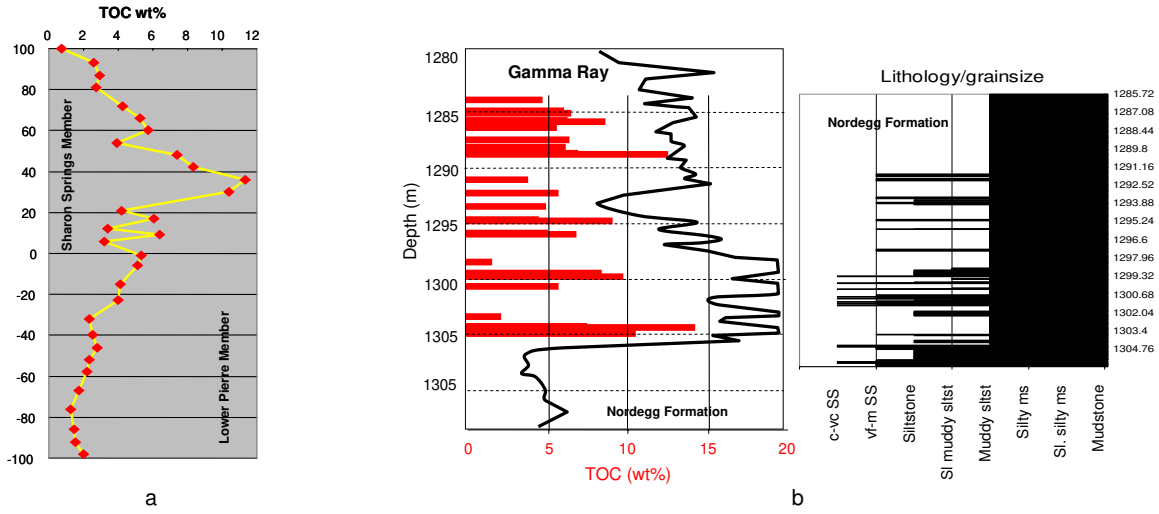

Figure 3 - a) Measured TOC profile indicating parasequence-set -scale stacking patterns of TOC in the Sharon Springs member of the Pierre Shale, Oral, South Dakota, USA. Note variations even in the interval of higher TOC values. (vertical scale in feet) b) Measured TOC profiles with grain size from core indicate high vertical variability within an overall organic-rich interval in the Nordegg formation in Alberta, Canada. The gamma-ray scale is 0 to 150 GAPI.

Interaction of processes: Although organic-matter enrichment can be expressed as a relatively simple relation, it is quite complex in detail because of the interdependencies of the variables:

Organic-matter enrichment = Production – (Destruction + Dilution)

where: Production = *f*(Nutrient supply), Destruction = *f*(Production of organic matter) + *f*(Oxidant exposure time) – *f*(Clastic sedimentation rate < burial-efficiency threshold), and Dilution = *f*(Clastic sedimentation rate > burial-efficiency threshold) + *f*(Production of biogenic silica or carbonate relative to protoplasm) (Bohacs et al., 2005). As the system of Equations 1, 2, and 3 indicate, the accumulation of organic matter is ultimately the result of competing rates: it is essential to produce organic matter faster than it is consumed or oxidized. Observations of many organic-matter-rich rocks ranging in age from Cambrian to Recent indicate that ORRS accumulate in a variety of settings and result from appropriate combinations among competing rates of production, destruction, and dilution of organic matter (e.g., Potter et al. 1980; Arthur et al. 1987; Huc 1988, 1995; Katz and Pratt 1993; Ricken 1993; Schwarzkopf 1993; Tyson 1995, 2001; Bohacs 1990, 1998; Werne et al. 2002). There are many combinations that can yield rocks enriched in organic material, especially for moderately rich potential source rocks that can serve as shale-gas reservoirs (Bohacs et al., 2005, their Table 1).

Stratigraphic Variations of Shale-Gas Reservoir Potential at Sequence and Parasequence Scales

Even within an overall background of favorable conditions for accumulation of organic matter, the properties and distribution of potential source rocks vary systematically at several vertical and lateral scales, from lamina to super sequence, spanning tenths of millimeters to thousands of meters (Bohacs, 1990, 1993, 1998; Schwalbach and Bohacs, 1992; Creaney and Passey, 1993; Bessereau and Guillocheau, 1995; Bohacs et al., 2005). These systematic variations are controlled by depositional environment and stratal stacking. Depositional processes intrinsic to the environment form lithofacies packages and stratal surfaces that are the basic building blocks of the geologic record. Extrinsically controlled accommodation stacks these facies building blocks into a nested stratal hierarchy. Each major physiographic setting accordingly accumulates characteristic vertical and lateral distributions of lithofacies recorded in their stratal stacking, mineralogy, and organic-matter content and character. These characteristic lithofacies distributions are recorded in quasi-periodic, parasequence-scale packages that stack systematically to form depositional sequences whose expression varies significantly within the marine depositional realm.

Sequence-scale variations: The marine realm includes three physiographic settings that accumulate significant organic-matter-rich rocks: constructional shelf margin, platform/ramp, and continental slope/basin (Bohacs, 1998). At the sequence scale in constructional-shelf-margin settings (Figure 4a), organic-carbon content generally increases in each parasequence up to the maximum-flooding downlap surface and then decreases step wise. In this setting, shoreline clastic dispersal systems are directly coupled to the basinal depositional areas. The result is the deposition of parasequences that tend to decrease monotonically in

thickness and increase in organic-matter content towards the basin; organic-matter type changes systematically from terrigenous, low-hydrogen content proximally to marine, high-hydrogen content distally. In contrast, in the platform/ramp setting (Figure 4b), parasequences are relatively thick in basinward positions and thin (or lap on) toward basin margins. The distribution of organic matter differs significantly from the constructional shelf margin: the platform/ramp setting shows little or no organic-facies changes towards the limit of fine-grained deposition (Grabowski and Glaser, 1990; Wignall, 1991; Leckie et al., 1990; Bohacs, 1998; Guthrie and Bohacs, 2009). Maximum organic-carbon content occurs in the basal transgressive systems tract and decreases stepwise to background levels at the maximum-flooding downlap surface. The continental slope/basin setting occurs where distinct and significant relief develops (Figure 4c), due in large part to the transition from continental to oceanic crust (Vanney and Stanley, 1983). The position and bathymetry of this setting leads to strong interaction with open-oceanic currents and processes. Clastic dispersal systems are dominated by mass gravity flows and organic deposition by pelagic and hemipelagic sedimentation as well as by sediment-gravity flows. Relations among organic parameters and physical processes may differ significantly from those on continental shelves (Bohacs, 1990, 1993). Bathymetry and its effects on oceanic processes and circulation patterns strongly control the distribution of fine-grained sediments and the organic matter they contain.

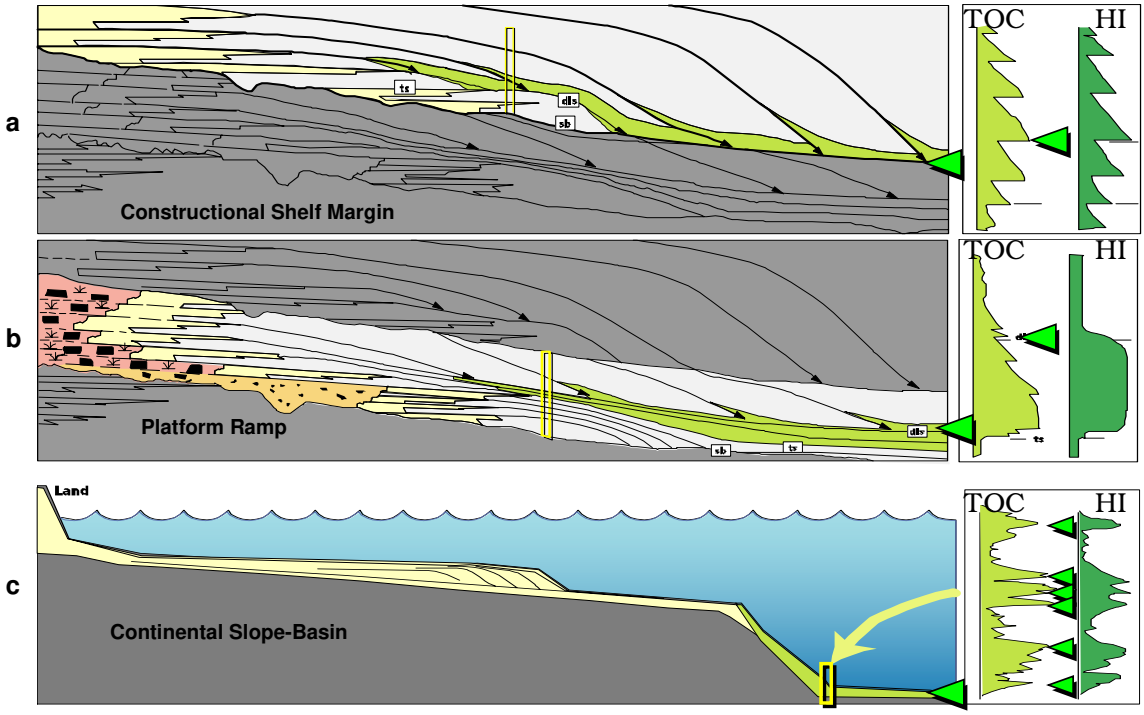

Figure 4 - Physiographic settings of the occurrence of organically enriched mudstone. a) Constructional Shelf Margin, b) Platform/Ramp, and c) Continental Slope-Basin. Also shown are typical TOC and HI stacking patterns for each setting. Vertical scale is meters to tens of meters.

Physiographic-setting-scale models provide the bridge between global and local controls on organic-matter accumulation, integrating global and derivative influences on the proximate controls of production, destruction, dilution, and accommodation. The various settings also provide a practical way to recognize key local controls and estimate the distribution and character of organic matter in a particular area. Hence, one looks at global reconstructions with an eye to areas favorable for the development of each particular physiographic setting (at the regional to basinal scale) and then uses parameters of the physiographic setting model to understand and extrapolate organic-matter-rich rock occurrences and character at the sub-basin to local scale. At any vertical section, however, significant changes in the mudstone properties occur at parasequence and parasequence-set boundaries (Miskell-Gerhardt 1989; Bohacs 1998; Bohacs et al., 2005). These changes are discussed in the following section.

Parasequence-scale variations: The basic stratigraphic building block in essentially all ORRs is the parasequence or its equivalent: a relatively conformable succession of genetically related beds or bedsets bounded by flooding surfaces or their correlative surfaces. Parasequences are typically meters to tens of meters thick and extend over significant portions of a basin, on the order of hundreds to thousands of square kilometers. In marine shelf or lacustrine settings, they typically represent one episode of shoreline progradation. They are interpreted to form in centuries to millennia.

Rock properties vary vertically at each well or outcrop location in a systematic manner that is related to the accumulation of the entire parasequence stratal unit (Figure 5a, 5b). Systematic changes in rock character laterally also occur, as a function of proximity to sediment supply points (typically the shoreline; Guthrie and Bohacs, 2009).

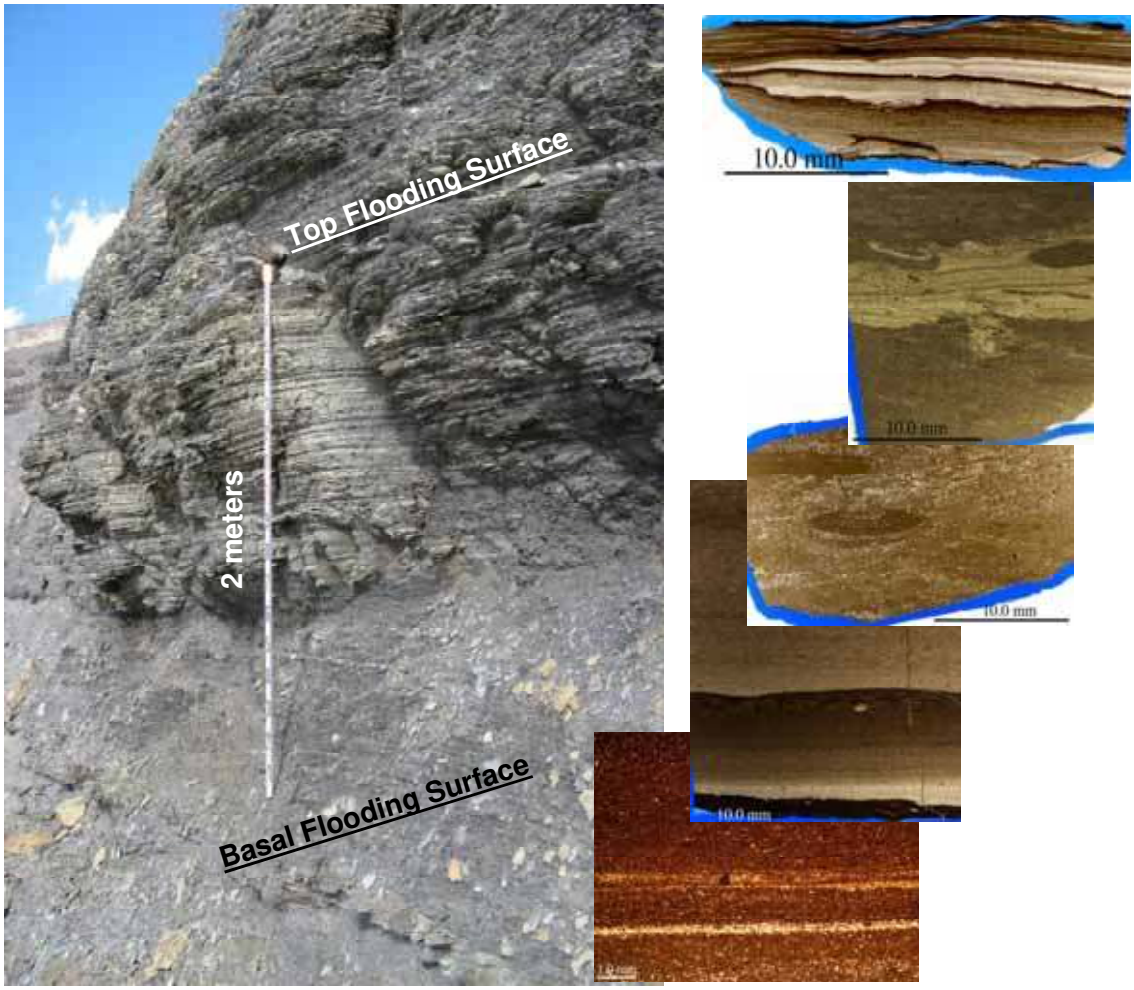

Figure 5a - Representative variation in sedimentary structures typically observed in a single parasequence deposited in a distal setting, such as this 2-meter thick one in the Cretaceous Mowry Shale, near Vernal, Utah, USA.

Proximal areas: In relatively proximal shelf areas, parasequences are 1- to 10-meter-thick coarsening-upward stratal units, defined by lithologic indices: percent sandstone, maximum grain size, thickness of individual sandstone bedsets (Figures 6a). These parasequences also demonstrate an upward increase in skeletal phosphorus content and bioturbation along with an upward decrease in total-organic-carbon content and radiolarian abundance (Figure 6a). A typical parasequence starts at base in laminated very dark grey claystone, with sparse millimeter-thick silt beds and thin lags of skeletal phosphate. The thickness of the siltstone or very fine sandstone beds gradually increases to centimeter scale; these beds commonly have planar-parallel or current bedding and horizontal burrows. Upward, sandstone beds more commonly have erosive bases and fining-upward trends, but are still interbedded with mudstone. Horizontal burrowing increases in intensity upward. Within these parasequences, the enclosing mudstones become siltier and more intensely bioturbated, upward, with minor vertical burrowing along with dominantly horizontal burrows. At the top of the parasequence, sandstone beds become coarser and more common, with very thin intervening mudstone. Sandstones tend to be dominated by current lamination or intensely bioturbated with both vertical and horizontal burrows, commonly from the mudstone of the overlying parasequence. Along with increasing bed thickness, grain size increases within the parasequences, from silt to about 0.125 mm. In the same interval, phosphorus content can double and then decrease in the relatively sandy parasequence top

Figure 5b - Example of organic-richness vertical profile and flooding contact in a relatively proximal setting, Exshaw type section, Jura Creek, Alberta, Canada. The flooding surface is marked by the light blue symbol (see inset for detail of this contact), and various parasequence packages are indicated by the breaks in the weathering profile and the TOC vertical variability. A correlative surface and TOC profile are shown in Figure 15.

All attributes within parasequences in proximal sections record an increase in bottom energy and oxygen levels due to shoreline progradation and water-depth shallowing: grain size and sandstone percentage increase because the influence of storm currents becomes more frequent and stronger at the depositional site, phosphorus content rises due to concentration of fish debris by storm currents, TOC decreases because of increases in bioturbation (indicating emergence above a redox boundary), re-exposure and oxidation of organic matter by storm currents, and by an overall increase in grain size. These observations indicate shoaling and more proximal storm sedimentation upwards and a correspond increase in clastic sedimentation rates. The coarsening-upward trend is paralleled by increases in bioturbation and inorganic (skeletal) phosphate content, and decreases in TOC content and radiolarian abundance. The overall envelope of maximum TOC shows a peaked distribution relative to HI (Figure 6a; Bohacs et al., 2005): positively correlated where increasing maximum TOC is due to increased algal content with high inherent HI (in relatively distal environments) and inversely correlated where increasing maximum TOC is due to increased content of woody and coaly organic matter with low inherent HI (in relatively proximal areas). Radiolarian abundance decreases with shoaling because they are holoplanktonic and cannot tolerate the fluctuations of temperature, salinity, and turbidity that occur nearshore (Heckel 1972), suggesting a decreasing influence of these consumer organisms. All observations in proximal sections indicate that dilution processes are dominant in controlling enrichment in organic matter. This leads to the characteristic vertical profile of TOC referenced in the previous section and illustrated in Figure 5b.

Distal areas: In the most distal regions, parasequences are significantly thinner, and contain a larger proportion of laminated to parallel-bedded very dark gray claystone and mudstone than in proximal settings with few centimeter-scale storm layers (< 2% of the section). Lithologic indices still indicate an upward-shoaling trend: percent sandstone, percent siltstone, maximum grain size, thickness of individual sandstone or siltstone bedsets (Figure 6b). A significant portion of the silt- and sand-size particles tend to be biogenic (reworked radiolaria, coccoliths, etc.). These parasequences generally demonstrate an upward increase in skeletal phosphorus content, total-organic-carbon content, hydrogen index, and bioturbation and a slight decrease in biogenic silica abundance (Figure 6b).

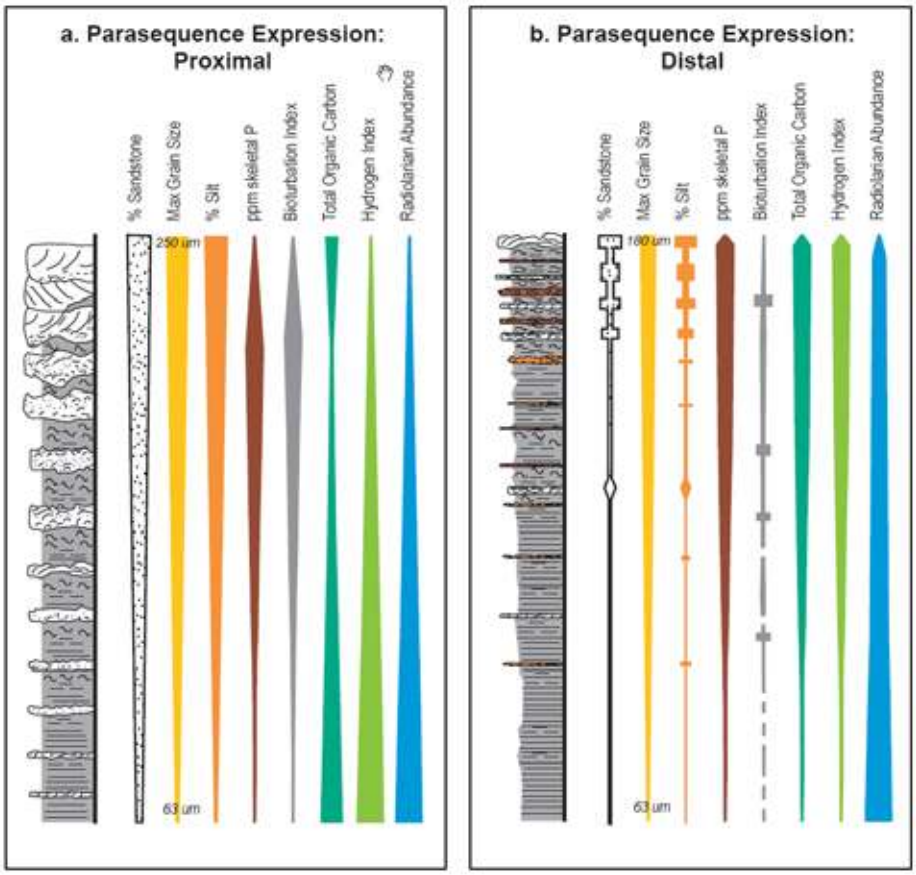

Figure 6 - Schematic comparison of parasequence expression in proximal (a) and distal areas (b), based on studies of the Mowry Shale. Proximal settings appear to be controlled mostly by clastic dilution and bottom energy conditions; distal setting mostly by primary organic production, with minor influence of biogenic dilution processes

A typical distal parasequence starts at base in parallel-bedded very dark grey claystone, with very sparse millimeter-thick silt beds and thin lags of skeletal phosphate and microfossils. Siltstone beds gradually become more common and increase in thickness to centimeter scale; these beds commonly have planar-parallel or current bedding and horizontal burrows. Upward, burrowing increases in intensity and diversity with subordinate vertical burrowing along with dominantly horizontal burrows. At the top of the parasequence, microfossil lags and siltstone beds are more common, with intervening mudstone to silty mudstone. Biogenic silica or carbonate of pelagic origin becomes less abundant in the upper 10 to 20% of the parasequence whereas coarser-grained biogenic carbonate of benthic origin is commonly more abundant near the top.

Lateral changes and their controls: Parasequence sets in intermediate positions between proximal and distal areas commonly show a smooth transition upsection from one end-member parasequence type to the other. This smooth transition in the basal transgressive systems tract from proximal parasequence type to distal parasequence type records a relatively abrupt transgression into a position and water depth too far offshore to be influenced significantly by storm sedimentation and clastic supply. In a few other locations, TOC and phosphorus signals can decouple, suggesting transgression into water depths too distal for clastic storm sedimentation, but not deep or distal enough (or into the right location) to be controlled by production changes (Bohacs et al., 2005).

The patterns of changes in organic-matter enrichment from proximal to distal settings within coeval strata appear to be due to changes in the relative importance of organic production, destruction, and dilution. In proximal areas, TOC content peaks in the uppermost transgressive systems tract, the interval with the lowest total accumulation rate, and shows a strong inverse relation with clastic-detritus content (Figure 7). These observations, along with the relations of TOC to P, BI, and HI, indicate that dilution rate is the dominant control in proximal areas. This agrees with the sequence-stratigraphic model of Creaney and Passey (1993) that demonstrated the signature of progradation in organic-matter enrichment at the parasequence and depositional-sequence scale. In distal areas, total and clastic accumulation rates are significantly smaller than in proximal areas (by factor of 2 or more), whereas

relative rates of biogenic silica accumulation are mostly greater (up to 47% in some units), especially in the uppermost portion of the highstand systems tract (Figure 7). These relations, along with the positive correlation among TOC, P, HI, and bioturbation index, indicate that primary organic production is the dominant control in distal reaches. Dilution by biogenic silica plays a secondary role, but appears to be a factor in the displacement of the TOC peak to above the maximum flooding downlap surface, to an interval with abundant to very abundant concentrations of biosilica and clay minerals.

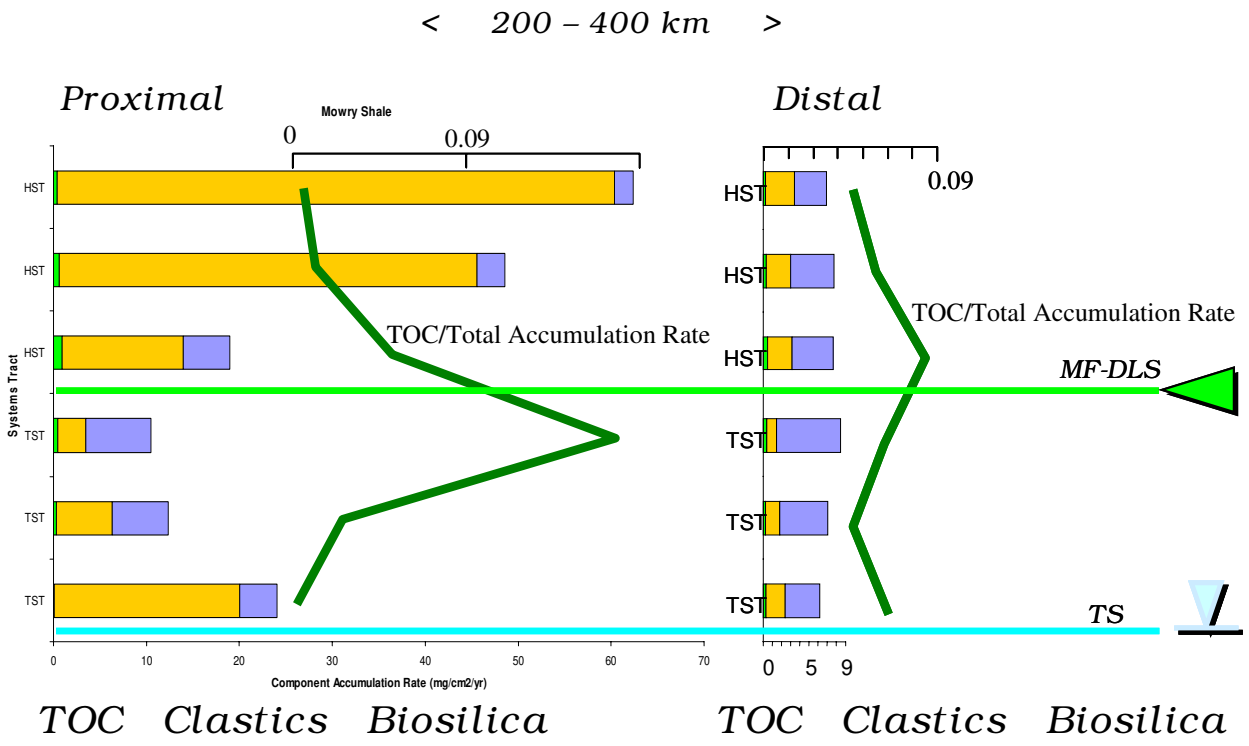

Figure 7 - Comparison of vertical and lateral changes in component accumulation rates (after Bohacs et al., 2005). Note the wide range of clastic dilution in proximal column compared to dominance of biogenic production in distal column.

In summary, dilution appears to be the main control in proximal areas, whereas production is dominant in distal regions. These scales of change highlight the necessity of considering the three-dimensional distribution, changes, and interplay of production, destruction, and dilution processes and their relation to local accommodation to understand fully any particular ORR or potential shale-gas unit. Detailed sequence-stratigraphic analysis reveals genetically related rock units and enables the application of process-based models to understand and predict the occurrence, distribution, and character of ORRs that serve as shale-gas reservoirs. This framework can be scaled from basin-wide formations to field- and flow-scale units (Guthrie and Bohacs, 2009; Bohacs and Lazar, 2010). The detailed stratigraphic framework is essential for relating detailed rock-property measurements to bulk flow behavior (discussed in the following sections), for scaling up to construct reservoir models, and for estimating resource density and distribution.

Organic-matter Type and Maturity

Most current shale-gas reservoirs had their origin as organic-rich mud. These sediments could have been deposited in the marine environment, in lakes (lacustrine), or in associated swamps and mires along the margins of lakes or seas. The type of organic matter deposited, and ultimately preserved in the mud, depends on the environment of deposition. Organic geochemists (e.g., Tissot and Welte, 1984) have used hydrogen-to-carbon and oxygen-to-carbon ratios to describe the various types of organic matter (or kerogen) in organic-rich mudstones that have generated much of the oil and gas that resides in conventional reservoirs worldwide; Type I and Type II kerogen are from algal and herbaceous material, have high H:C ratios, and will typically generate oil during the thermal maturation phase associated with burial, time, and temperature; Type III kerogen is largely composed of woody/coaly material and will generate mostly gas during thermogenic maturation. If hydrocarbons are generated from these rocks, they are termed “source rocks”.

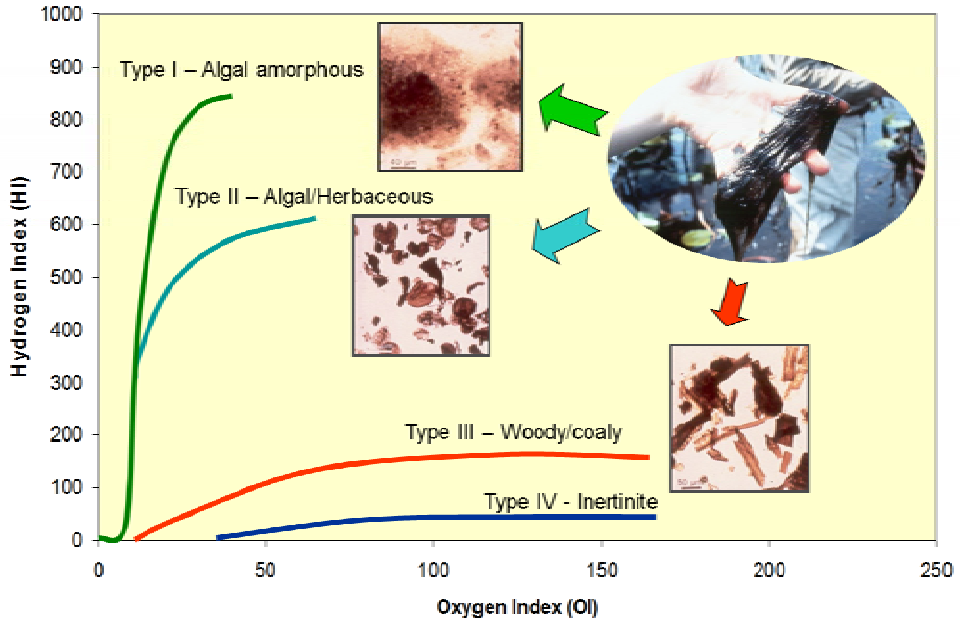

Figure 8 - Principal types and evolution paths of kerogen are shown on this van Krevelen diagram: Types I, II, and III are the most frequent. Kerogens of intermediate composition also occur (after Tissot and Welte, 1984).

The critical parameters related to whether or not a given rock will be a good source rock is the organic richness (generally recorded as wt% Total Organic Carbon – TOC), the current and past maturity level of the formation (generally referenced as Vitrinite Reflectance, Ro), and the organic matter type (whether the primary thermogenic product will be oil, gas, or a mixture). During the deposition of these organic-rich muds, a variety of geologic and biologic processes contribute to the concentration of organic matter ultimately preserved in the rock, as described previously.

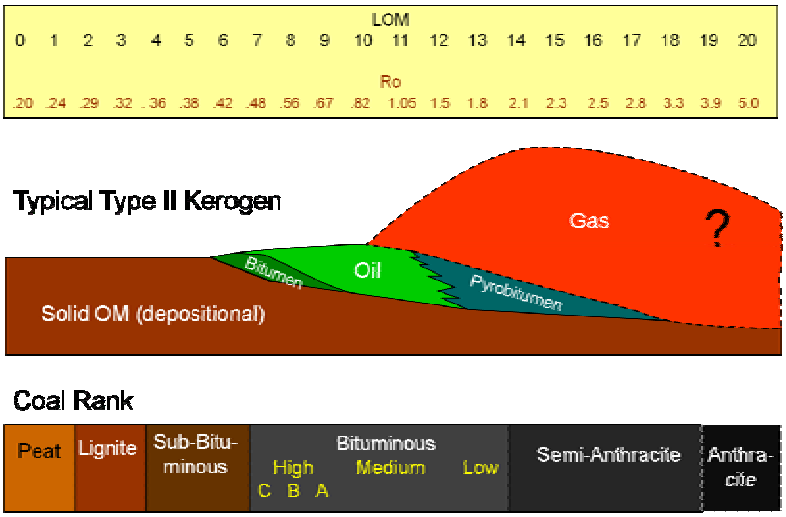

Figure 9 - Schematic of maturation of a Type II (oil-prone kerogen) compared to coal rank. Also, shown are the respective maturity in LOM units (Level of Organic Metamorphism; Hood et al., 1975) and corresponding vitrinite reflectance (Ro).

During the exploration phase for hydrocarbons, the location (depth and lateral extent) of these organic-rich formations is critical for understanding the complete hydrocarbon system that may, or may not, be present in a sedimentary basin. The current and past depth of burial and heat flow history provides critical information on the timing of generation and expulsion of hydrocarbons to conventional traps. The principal generation windows for oil-prone kerogen (Type I and Type II) ranges from Ro=0.5 (for early generation) through peak generation Ro=0.8, to overmature Ro>1.1. Above Ro=1.1, any residual oil or oil-prone kerogen will

likely be cracked to gas. The current targets for shale-gas reservoir exploration are overmature oil-prone source rocks; thus, unconventional shale-gas reservoirs are simply highly mature organic-rich rocks that have gone through primary thermogenic maturation, but have retained sufficient residual gas to be of economic interest. The key may be how and where that gas is stored, as described below.

Why Total Organic Carbon (TOC) is Important in Shale-Gas Rocks

Because of the strong vertical heterogeneity observed in source rocks (Figures 3, 7), it is expected that these same variations exist in the overmature expression of these source rocks as shale-gas reservoirs. Examination of dozens of shale-gas formations worldwide clearly indicate that the total porosity and gas content (gas-filled porosity or bulk-volume gas BVG) is directly associated with the TOC content of the rock (Figure 10). Some reasons behind these relations will be discussed later in this paper, but sufficient to state that high local TOC is a critical factor to assess when evaluating potential shale-gas reservoirs because it relates to both porosity and gas saturation.

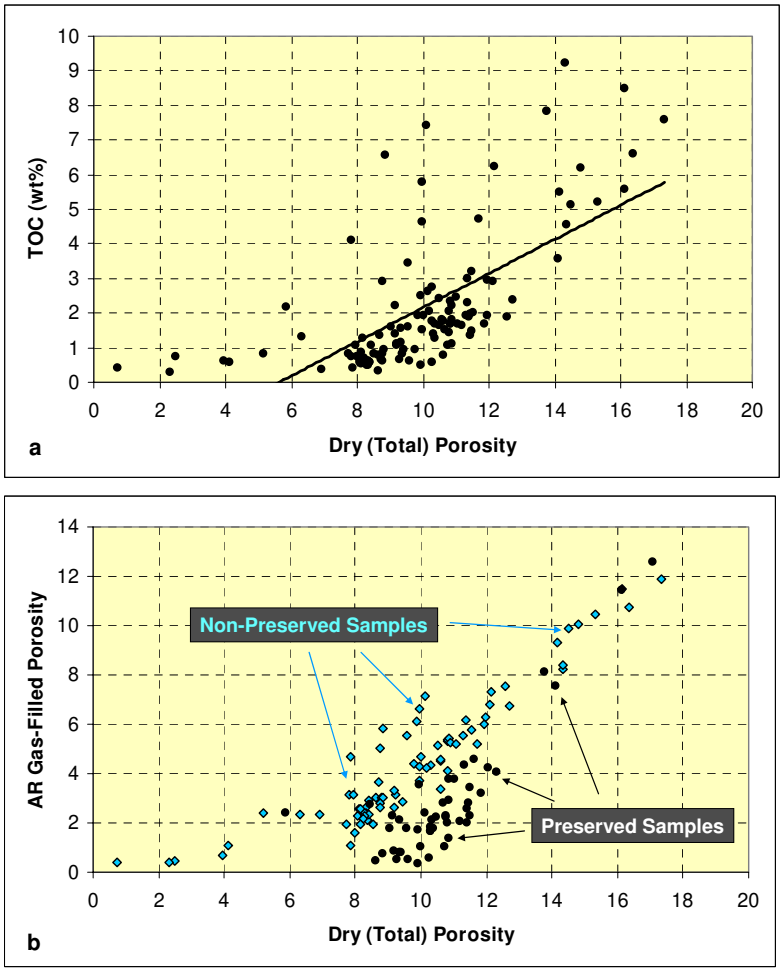

Figure 10 – a) Relation between Total Porosity (p.u.) and TOC (wt%); b) relation between Total Porosity (p.u.) and As-Received Gas-Filled Porosity (p.u.) for preserved and non-preserved samples. Preserved samples are recommended.

Analytical Characterization of Shale-Gas Rocks

Numerous geochemical and petrophysical techniques have been developed to characterize organic-matter-rich source rocks. Although most techniques were developed to characterize thermally mature source rocks in the oil-generation window, the same techniques can be applied, sometimes with modification, to the shale-gas class of unconventional reservoirs that currently exhibit maturities much higher than the onset of overmaturity (i.e., Ro>1.1). Typical sample analytical techniques include: TOC, X-ray diffraction (XRD), adsorbed gas analysis, vitrinite reflectance (Ro), detailed core description, thin section petrography, and electron microscopy. These results are combined with a full suite of well logs, including high resolution and borehole imaging logs, to best characterize these heterogeneous formations. Characterization of porosity, fluid saturation, and permeability derived

from core can be tied to log response, but several studies have shown that the results obtained from different commercial core analysis laboratories can vary significantly (as discussed later in this paper; see also Sondergeld et al., 2010b). Thus, the "ground truth" characterization easily available for conventional sandstone reservoirs, is somewhat less certain in these mudrocks.

Mineralogical variation in Shale-Gas Reservoirs - Mineral composition in shale-gas reservoirs varies widely. Figure 11 is a ternary plot based on quartz, total clay, and total carbonate with the compositional fields outlined for the Barnett and Eagleford plays in North America, contrasting with the composition of a clay-rich gas-bearing mudstone. As can be seen, the compositional variations span nearly the entire compositional field of this plot. Current producing plays tend to lie below the 50 % clay line. The shale-gas plays that contain greater than 50 wt% quartz or carbonate tend to have a more brittle character that responds well to current well stimulation practices.

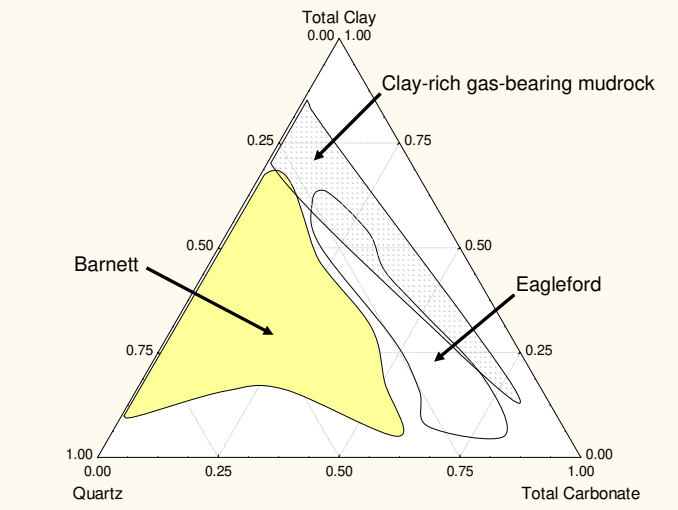

Figure 11 – Mineral composition is quite variable in each shale-gas reservoirs.

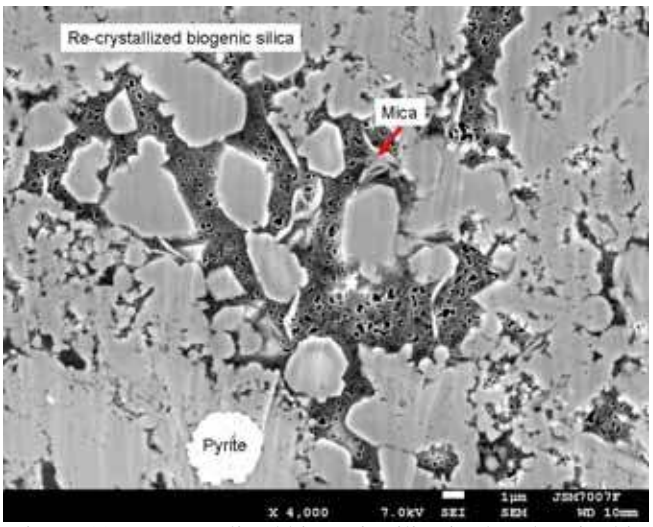

Figure 12 - Recrystalized biogenic silica is abundant in this Barnett sample. The porosity in the organic-matter is discussed later in this paper.

From a stimulation perspective, not all quartz is created equal in shale-gas reservoirs. The most effective quartz component appears to be recrystalized biogenic opaline silica (Jarvie et al., 2007) that forms a continuous framework of quartz cement, as shown in Figure 12.

Detrital quartz, on the other hand, appears to be less effective. Thyberg et al. (2009) provide evidence that extra-basinal detrital quartz is cemented by silica from smectitic-clay illitization during diagenesis according to the reaction:

$$\text{Smectite} + K^{+} = \text{Illite} + \text{Silica} + H_20 \text{ (Boles and Franks, 1979)} .$$

Thyberg et al. (2009) show evidence that such a reaction increases the brittle behavior of shales, but to date we have not observed this play style for enhancement of brittle behavior in shale-gas reservoirs. Extra-basinal detrital quartz may be more effective where it forms interbedded tight-gas sandstone plays associated with sediment entry points into a basin.

Mineralogical variation in shales not only occurs at the meter scale, but also occurs down at the mm to cm scale. Figure 13 is a thin section photomicrograph from a mudstone illustrating mm-to-cm scale thin beds of clay-rich and carbonate-rich end-member lithologies, spanning the clay-rich compositional field in Figure 11. Vertical lithological heterogeneity in shales appears to generally exceed that found in many sandstones.

Because the organic matter that becomes kerogen is deposited at the same time as the inorganic rock mineral grains, it is important to keep in mind that the volume occupied by the kerogen occupies a much larger volume percent (vol%) than is indicated by the weight percent (wt%) measurement; this is because of the low grain density of the organic matter (typically 1.1-1.4 g/cc) compared to that of common rock-forming minerals (2.6-2.8 g/cc). The impact of this is illustrated in Figure 14, which shows various scale scans of photomicrographs of relatively low maturity Woodford Shale (Ro=0.58, LOM=8). In this case the TOC of the sample was 20.9 wt%, but the corresponding volume percent of the kerogen is closer to 40% of the rock. Thus, relatively small amounts of wt% TOC have about double the impact on a volume % basis. This is important to remember because most well logs respond to volume percent quantities, as will be discussed below.

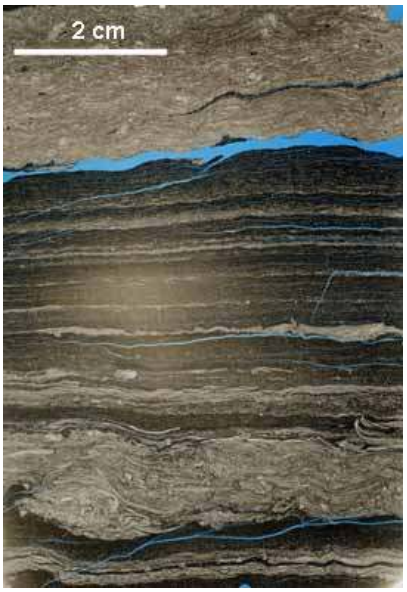

Figure 13 - Large-scale photomicrograph showing detailed bedding and composition variations on the sub-centimeter scale.

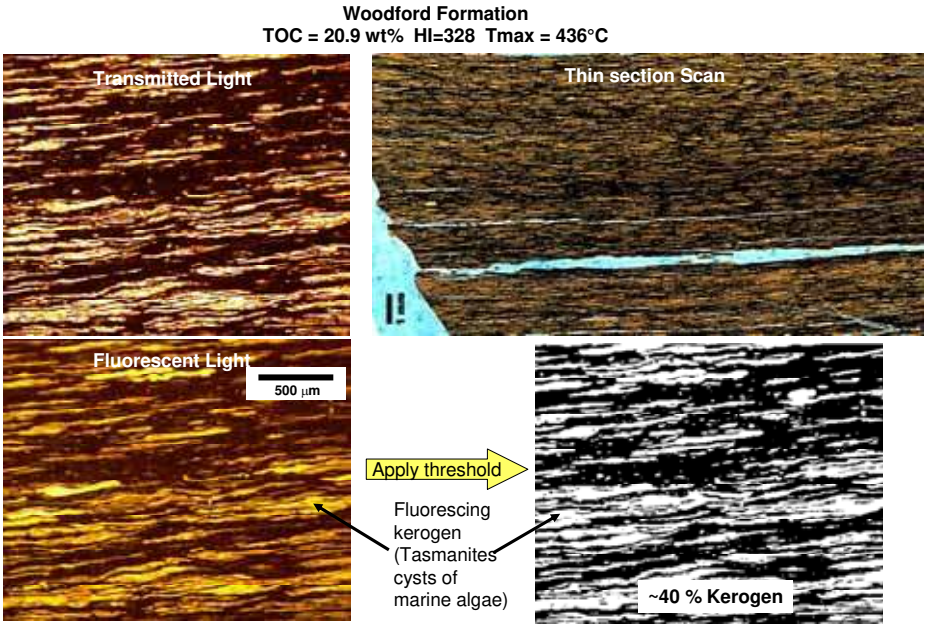

Figure 14 – Woodford shale thin section scan showing kerogen layers; note that 20 wt% TOC corresponds to about 40 vol% kerogen.

Well Log Response in Shale-Gas Rocks

Many of the well log techniques developed for mature oil-prone organic-rich rocks are readily applicable to the "overmature" shale-gas formations (for a more discussions of well log response in organic-rich formations see Passey et al., 1990, and Sodergeld et al., 2010b; Spears and Jackson, 2009). The main differences relate to the fluid type (gas instead of oil), distribution of porosity (occurrence of pores within the organic matter in addition to intergranular matrix porosity), and bulk rock composition (the presence or absence of brittle minerals in the rock matrix).

Gamma-ray and Spectral Gamma-ray – For most fine-grained rock evaluation the gamma-ray is a critical well log to help differentiate shales (seals or source rocks) from conventional reservoir lithologies, such as sandstone or carbonate. For shale-gas plays, the source, seal, and reservoir are often contained completely within the fine-grained rock lithofacies and the gamma-ray curve may or may not be as useful as in conventional reservoirs. If the shale-gas of interest is deposited under marine conditions (primarily Type II kerogen), the uranium content continues to be useful given its association with organic matter, and the uranium component can be a good indicator of organic richness. In lacustrine (or lake) settings, there is generally a paucity of uranium in these systems, and more often than not there is no relation between uranium and TOC (Bohacs and Miskell-Gerhardt, 1998; Bohacs, 1998); in these cases, the total gamma-ray curve remains a fairly good indicator of overall clay content in the rock (Bhuyan and Passey, 1993) but may not indicative of high TOC or the reservoir facies of interest. Figure 15 shows how the base of a parasequence is organic rich (decreasing upward), and this same observation can be seen in the total gamma-ray response.

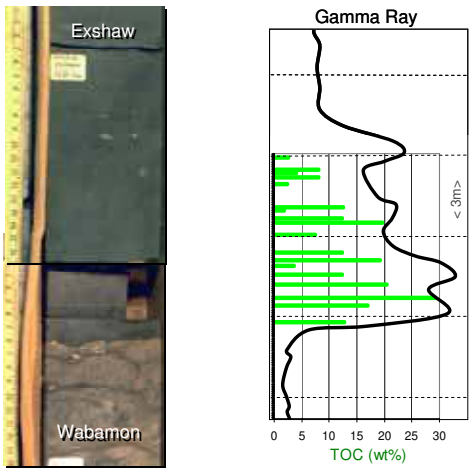

Figure 15 – Core photograph of Exshaw flooding surface; corresponding GR and measured TOC profile. Gamma-ray scale is 0 to 150 GAPI. See also Figure 7b.

Resistivity – The resistivity of a rock is directly related to those components that are electrically conductive. In conventional reservoirs, formation water is the primary conductor of electricity, at least when the formation waters are brackish to saline, allowing for ionic conduction. Low resistivity is observed when the amount of saline water-filled porosity is high – the larger the

volume of formation water (Bulk Volume Water), the lower the resistivity of the fluid-filled rock. Hydrocarbon fluids (oil or gas) are non-conductive, and when they are present in sufficient quantities, they displace the amount of water in a given formation, resulting in resistivity values higher than the same rock fully filled with electrically conducting formation water (Archie, 1942). There are many variants to the interpretation of resistivity in conventional reservoirs (e.g., clay conductivity and shaly sand analysis; thin-bed effects due to interbedded shales; Waxman-Smits, 1968; Worthington, 1985; Passey et al., 2006) but these are beyond the scope of the current paper, yet may play second-order roles in the quantitative interpretation of shale-gas reservoirs.

Many shale-gas reservoirs contain relatively minor amounts of clay (20-30 wt%), whereas others may contain as much as 70 wt% clay. The importance of additional clay conductivity on the interpretation of fluid saturation depends on the relative conductivity of the clay to that of the formation water; in general, if the salinity of the formation water is greater than the salinity of sea water (e.g., 35 kppm NaCl equivalent), then the relative impact of excess conductivity due to clay minerals is small. Moreover, the amount of water-filled porosity (i.e., bulk volume water or BVW) plays a role on the impact of clay conductivity, because with decreasing amount of conductive formation water (i.e., low porosity), the relative impact of clay conductivity to that of the formation water will increase.

Other minerals (organic and inorganic) also play a role in the overall conductivity of the rock (Anderson et al., 2008). Pyrite is commonly present in organic-rich intervals of shale-gas formations (due to the reducing conditions that enhanced organic matter preservation, as discussed in the first section) and may play a role in decreased resistivity response if the volume is sufficient, In general, most organic-rich intervals contain some pyrite, but overall, the resistivity remains relatively high in the TOC-rich intervals. As with organic matter, the matrix density of the rock components must be factored in when determining the volume percent occupied by that component. Due to the high density of pyrite, a rock containing 10 wt% pyrite may contain only 7 vol%, whereas with low density organic matter, 10 wt% TOC may correspond to about 20 vol% kerogen.

Finally, in some shale-gas reservoirs that are at very high maturities (Ro>>3), the overall rock resistivity can be 1-2 orders of magnitude less than is observed in the same formation at lower thermal maturities (Ro between 1 and 3). It was thought that perhaps the carbon in the organic matter is recrystalizing to the mineral graphite, which is electrically conductive, but preliminary studies indicate that pure mineral graphite (as indicated by XRD) is not present in abundance at these thermal maturities.. Thus, it is likely that a precursor to graphite is forming, and further studies are warranted. It is sufficient to state that in extremely high maturity organic-rich rocks (Ro>3), the rock may be much more electrically conductive due to other mineral phases being present rather than solely formation water, clay, and pyrite (as usually considered).

Density – Due to the low grain density of organic matter (or kerogen) the presence of organic matter can have a significant impact on the bulk density of the sample, and, consequently, on the bulk density measured by well log tools (Meyer and Nederlof, 1982; Passey et al., 1990). If there are no large local variations in other parameters that can affect the bulk density, then the density log can be used to build fairly robust proxies for TOC. One advantage of the density log is its relatively fine vertical resolution (~ 1 ft) that can be used to differentiate subtle and closely spaced vertical variations in TOC. This is extremely valuable when combined with high-resolution resistivity logs (as in the modified ΔlogR approach described below).

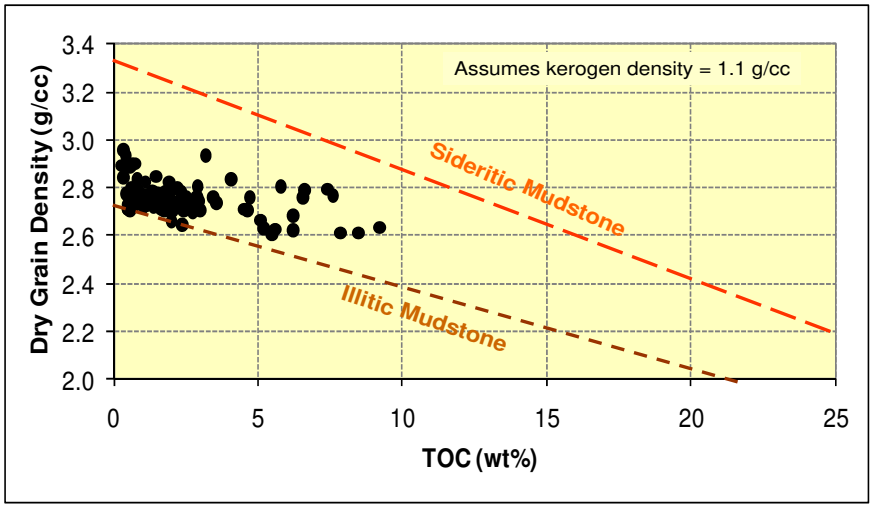

Figure 16 – Relation between TOC and dry grain density for samples from an illite clay-rich organic-rich mudstone . Also, shown are the theoretical limits for siderite-rich and illite-rich mudstones assuming the kerogen grain density is 1.1 g/cc,

Sonic – Similar to the density log response, the P-wave log can be calibrated to TOC content due to the low P-wave velocity (high transit time) of organic matter, given the previous caveats about no significant local variations (such as changes in porosity or mineralogy) that can affect sonic response. Most work to date has focused on the compressional (P) wave, but there is also a likely impact on the shear (S) wave response (Zhu et al., 2010). In general, the use of the sonic log for determining TOC is enhanced when combined with other logs.

Neutron – General observations are that the neutron log is a poor indicator of organic matter as a single stand-alone tool. This tool is affected not only by the hydrogen in the organic matter, but also by the hydrogen in the hydroxyl (OH^-) in the clay minerals (see Figure 20), as well as by the hydrogen in the formation water and any liquid or gaseous hydrocarbons present. For some silica-rich shale-gas formations, the use of the standard neutron/density overlay has proven useful for recognition of intervals that contain higher gas volumes; this technique has limited application when the formation is not clay rich, due to the increase in hydroxyl (OH^-) ions resulting in a larger neutron/density separation that may mask the "gas crossover".

NMR – Published applications of use of NMR logs for unconventional reservoirs evaluation are limited (e.g., Jacobi et al, 2009; Merkel and Gegg, 2008). In water-saturated low TOC shale-gas intervals, there is good agreement between total NMR porosity and total porosity measurements of core (using crushed rock methods). Further work is warranted to fully understand the response in organic-rich, and presumably, gas-bearing intervals.

Calibration of Logs to Total Organic Carbon Content

As has been shown for Type II (oil-prone) source rocks in the oil-maturity window (Ro=0.5-1.1), the presence of the organic matter and the presence of generated hydrocarbon fluids can have a large response on the resistivity log (Passey et al., 1990). At the time that work was done, the focus was entirely on the oil-mature window and limited data existed for overmature shale-gas rocks (i.e., Ro>1.1). Active exploration of shale-gas plays has allowed acquisition of the data required to calibrate the logs to many of the critical controls for successful shale-gas plays.

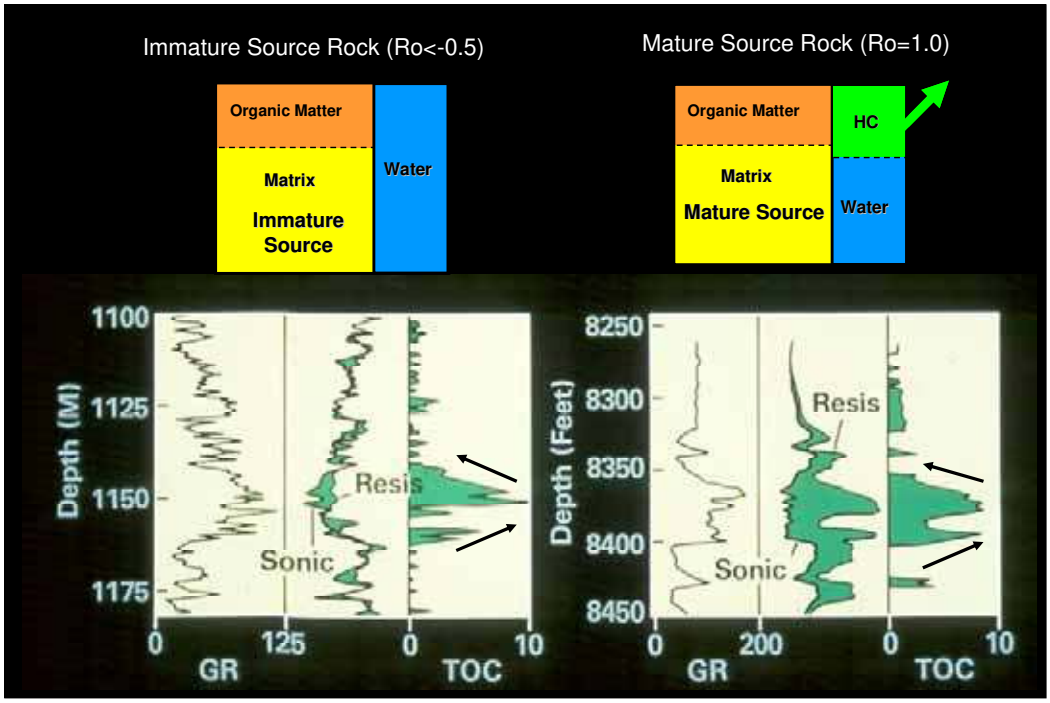

Figure 17 – Well log response (ΔlogR and GR) response for immature (Ro=0.5) and mature (Ro-1.0) Devonian age Duverney formation in Canada. Note that the parasequence-set scale packages are identifiable in the TOC profiles (black arrows).

Combined porosity/resistivity methods (e.g., ΔlogR method) – As described in the Passey et al.(1990), the original calibration of the ΔlogR technique (using either sonic-resistivity or density-resistivity combinations) was for source rocks in the oil maturity window (Ro = 0.5–0.9 or LOM 6-10.5). No rock calibration was available at that time to included rocks in the overmature or "gas" window (Ro > 1.0; see Fig. 9). As previously published, a parametric fit was made for TOC from ΔlogR separation as a function of LOM (maturity); the lines for maturities greater than LOM=10.5 (Ro>0.9) were numerical extrapolations of the lower maturity

calibration lines. Recently acquired TOC data from shale-gas formations worldwide indicate that for overmature intervals (LOM>10.5 or Ro>0.9) the calibration to TOC is the blue line (Figure 18). Use of the original Passey et al., (1990) "calibration" lines for rocks with maturity values LOM>10.5 (or Ro>0.9) will result in underestimation of the actual TOC. Sondergeld et al. (2010b) propose using a correction multiplier to obtain accurate log-derived TOC using the ΔlogR technique for overmature shale-gas formations, which is approximately equivalent to using the blue calibration line shown in Figure 18.

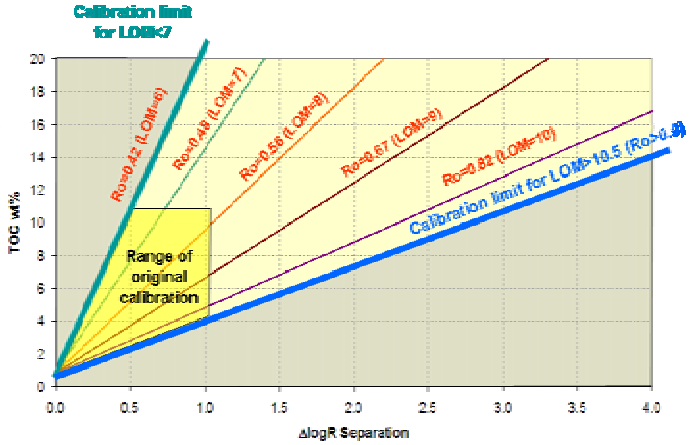

Figure 18 – Revised relation of ΔlogR to TOC indicating possible upper limit for rocks with LOM> 10.5 (Ro>0.9)

A comparison of ΔlogR-derived TOC with high-frequency measured TOC is shown in Figure 19a; the green shading represents the TOC from standard ΔlogR (sonic/resistivity) using the blue calibration line illustrated in Figure 18; the cyan curve in Figure 19a is TOC from the ΔlogR density/resistivity pair, and the orange line is from high-resolution density/resistivity logs, providing more detailed vertical variability of TOC, and comparable with the borehole electrical image log (Figure 19b).

Elemental and Mineralogic Logs – These logs can determine reasonable values for total clay, carbonate, and quartz (at least within ± 5-10 wt%), but none of these parameters are directly related to organic richness of shale-gas reservoirs. But, the total silica or total carbonate content is likely related to geomechanical properties of the rock. Moreover, these logs appear to be useful in identifying pyrite and/or siderite intervals, and these intervals are commonly associated with sequence-stratigraphic surfaces in distal environments where clastic input is minimized (Figure 4). Further analysis is warranted in using these logs for recognition of significant stratigraphic surfaces.

Borehole image logs – High-resolution borehole electrical images are useful for identifying closely spaced vertical variations in resistivity, which can be tied to variations in organic richness (possibly due to higher gas saturation in these intervals (Figure 19b). From this image, individual parasequences are readily identified -- high TOC and resistive (bright) at the base, and low TOC and conductive (darker) upward. Care must be used when interpreting borehole electrical images because tight (low porosity) carbonate or siliciclastic beds and siderite concretions appear resistive (bright).

The use of water-base mud is required for standard high-resolution electrical images. It may be possible to identify similar features using oil-base imaging logs, but the vertical resolution is likely to be coarser than for water-base-mud electrical imaging wireline logs.

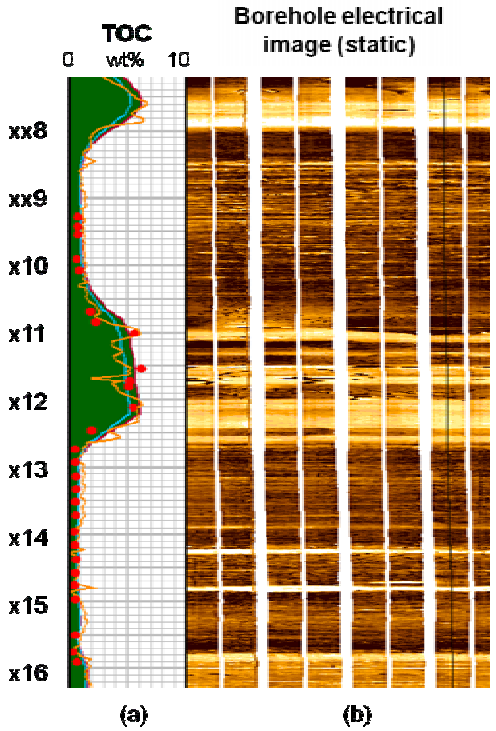

Figure 19 – a) Log-derived TOC using the ΔlogR approach showing comparison with high-frequency TOC core measurements. b) Static borehole electrical image log for the same interval as (a). Note the high-frequency variations in vertical properties and the parasequence expression (bright at base, darker upward).

Porosity in Shale-Gas Rocks

The nature of the porosity within overmature organic-rich formations may provide some insight into how they work, and into why analytical procedures for characterizing the porosity and fluids may vary. Within conventional siliciclastic reservoirs (e.g., sandstones), there is a clearer differentiation between intergranular porosity (between detrital grains) and secondary porosity within grains (intragranular porosity), such as microporous rock fragments, diagenetic clays, and partially dissolved detrital grains (feldspar, rock fragments). Once detrital clays and other very small particles are introduced, then the clear differentiation between what is fluid-filled porosity and what is solid is more complicated. The common clay minerals found in detrital systems are kaolinite, chlorite, illite, and mixed-layer illite-smectite (Figure 20). All clays have hydroxyls (OH^-) as part of their crystal structure; although the neutron log is affected by the hydroxyl, it is important to recognize that this is not water, or part of the total porosity of the rock. Only illite is inherently radioactive, although trace amounts of thorium can be found substituting in the crystal structure of montmorillonite-family clays. Because of the very small grain size of clays, a large amount of surface water is associated with clay minerals, either as adsorbed water, double-layer water containing electrically conducting cations, or as strongly held capillary-bound water (but beyond the standard "double-layer" of water) (Eslinger and Pevear, 1988). Sometimes, all these are collectively referred to as "clay-bound water" but their quantitative measurement and differentiation is problematic and imprecise, especially if one chooses to use water saturation (Sw) as an indicator of volumes of water.

Kaolinite - $Al_4[Si_4O_{10}](OH)_8$

Chlorite - $(Mg,Al,Fe)_{12}[(Si,Al)_8O_{20}](OH)_{16}$

Illite - $KAl_4[Si_7AlO_{20}](OH)_4$

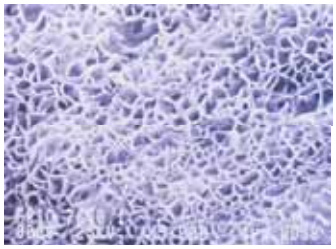

Smectite - $(Ca,Na)(Al,Mg,Fe)_4[(Si,Al)_8O_{20}](OH)_4 \bullet nH_2O$

Figure 20 – Four major clay types encountered in sedimentary rocks. Also, shown are their chemical formulae.

Most siliciclastic grains are water-wet indicating that there is a very thin layer (or double-layer) of water on the grain surfaces; for sandstones, the volume of this water is largely negligible compared to the volume of void space (the pore space) between grains. In fine-grained rocks, such as mudstones, the particle size is orders-of-magnitude smaller, and, thus, the surface area is orders of magnitude larger (Table 1, and Figure 21). In clay-rich rocks, the water related to the clay surfaces is significant relative to the total porosity; moreover, for some types of clays (the smectites/montmorillonites), there exists interlayer water that some consider part of the total porosity system, and others consider part of the crystal structure. The nature and bonding mechanisms for the surface water has been studied for decades, and is still a point of scientific discussion, the details of which are beyond the scope of the current paper (see Feibelman, 2010 for a discussion of the binding mechanisms related to the first layer of water on kaolinite).

Table 1 - Surface area of common clay minerals (and fine grain sandstone)

Clay Type	Internal Surface Area (m2/g)	External Surface Area (m2/g)	Total Surface Area (m2/g)
Smectite	750	50	800
Illite	0	30	30
Chlorite	0	15	15
Kaolinite	0	15	15
Fine Quartz Sand	0	0.02	0.02

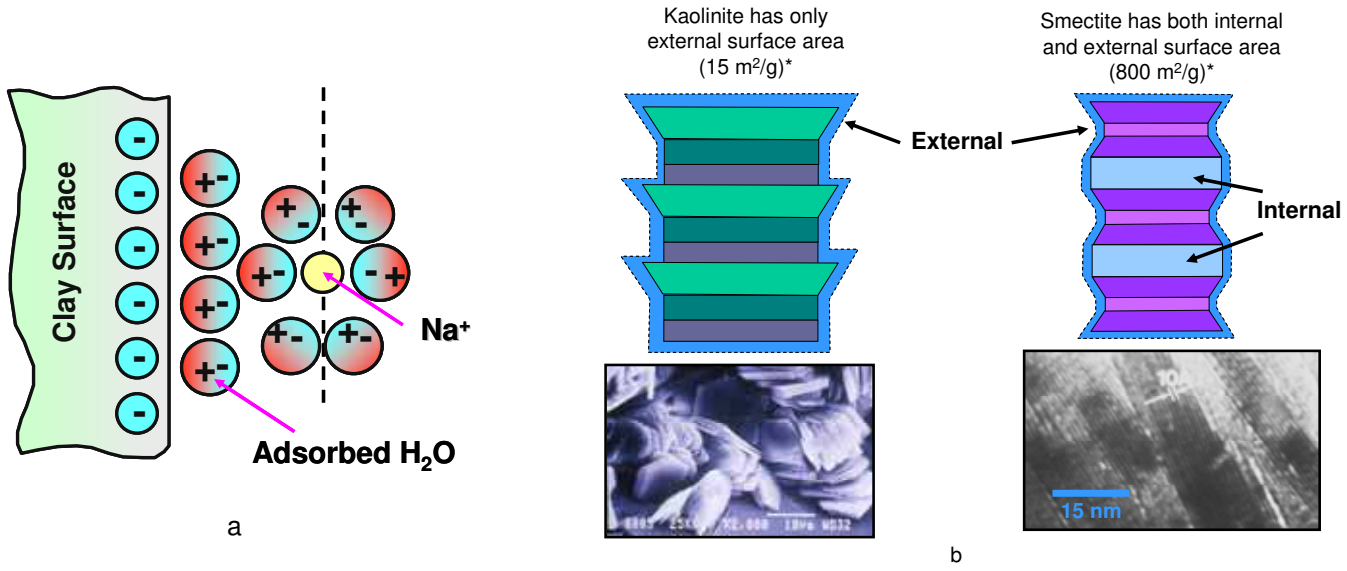

Figure 21 – a) Schematic of "adsorbed" surface water and double-layer of water. b) Schematic and SEM images showing that kaolinite has only external surface area and smectite has both external and internal surface area. The TEM (transmission electron microscope) image of the smectite shows that the collapsed layer (without water) is 10 angstroms, 1.0 nm).

For all clays, there exists yet another contributor to the confusion about definitions of porosity: the hydroxyl ion (OH^-) that occupies crystal lattice sites in the octahedral layer of most clays (Figure 22), but this ion is not actually liquid water and does not conduct electricity via ionic conduction. The hydrogen in the hydroxyl is, however, detected by the standard neutron logging tools and is the cause of the routine neutron-density separation noted in clay-bearing shales or mudstones.

In addition, interparticle porosity exists between clay grains, analogous to intergranular porosity in sandstones, but in clay-rich rocks, the pores are much smaller, due to the smaller grain sizes. The clay integranular pores are very small (likely with dimensions of 10's of nanometers), and although the dimensions are orders of magnitude greater than the surface water, capillary forces are likely great. The question arises if this capillary-bound water is part of the total porosity of the rock, or included as part of the "fuzzy" (poorly defined) clay-bound water term. The issue is compounded when porosity measurements are made on non-preserved rock samples.

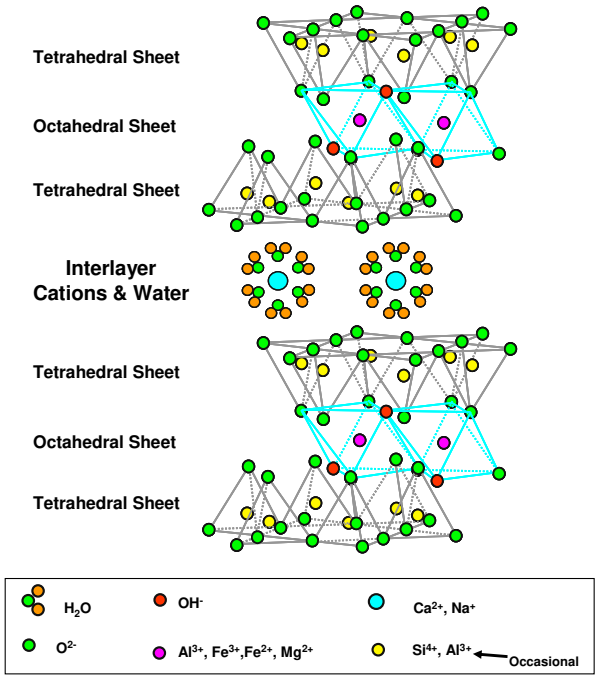

Figure 22 – Crystallographic structure of Smectite showing the occurrence of (OH^-) ions and interlayer water (after Grim, 1968).

Quantification of Porosity (comparison of various labs)

The method commonly used to measure porosity of gas shales is to crush the rock to a specific particle size and measure the grain volume of the crushed rock samples using a He pycnometer; it has been reported, however, that for dried samples, the measure of total porosity may depend on the molecule used for the measurement (Bustin et al., 2008). For crushed-rock porosity determination, the bulk volume of the intact sample is found prior to crushing, using volume displacement method in which the

sample is immersed in a fluid such as mercury. The details of the method are described in Luffel et.al. 1992, and Luffel and Guidry, 1992. We have observed significant disparities in the porosity values reported by different laboratories that use this method to measure porosity as shown in Figure 24a (see also Sondergeld et al, 2010b). The sample splits sent to the different laboratories were from the exact same sample depths to eliminate vertical variability. Some of the observed differences may be attributed to handling of these samples such as crushing the rock to different sizes and exposure of the samples to different environments.

As shown in Figure 23, a typical shale-gas rock volume is composed of matrix made up of inorganic minerals and organic matter, along with pore space between these components. One of the sources of disparity in the porosity values reported by different laboratories is likely because of the way the term "porosity" is defined and used. Some laboratories report a "total (dry) porosity" which is the pore space that holds the hydrocarbons, mobile water, and irreducible water composed of capillary and surface clay-bound water; whereas others report an "effective" or "humidity-dried" porosity that does not include the pore space occupied by the surface (or interlayer) "clay-bound" water. Unfortunately, the measurement of the "clay-bound" water may not be very accurate or precise due to variable definitions or conditions under which it is measured (e.g., temperature, humidity), rendering the term difficult to transform from a quantitative "effective" porosity to a quantitative "total" porosity. It is widely accepted that core analysis of conventional rocks must be carried out at reservoir stress since rock properties measured in absence of stress are quite different from measurements at reservoir stress. The crushed-rock methods used for shale-gas formations (Luffel et al., 1992) provide fast results for porosity measurements. Recall that porosity measurements carried out in the absence of reservoir stress can be different from in-situ porosity. The same holds true for gas-filled porosity measurements that are also carried out on crushed rocks in the absence of reservoir stress.

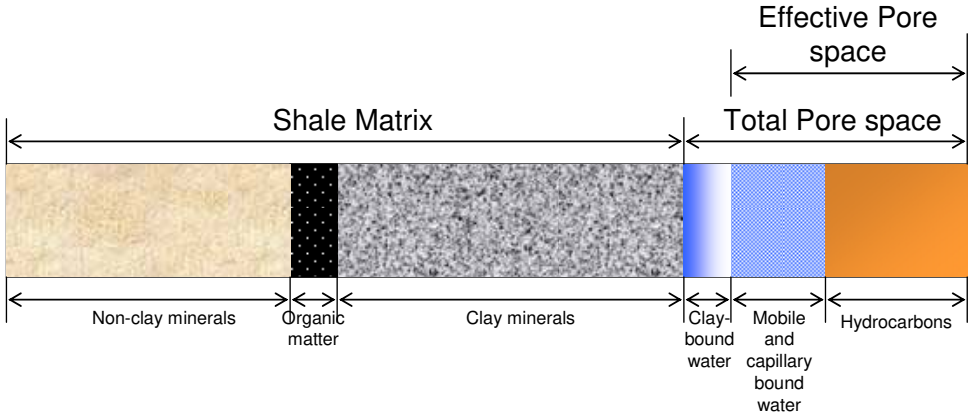

Figure 23 – Schematic of a clay-rich organic-rich rock solid, water, and hydrocarbons (modified after Eslinger and Pevear, 1988). Note that structural hydroxyl (OH^-) "water" is not considered here because it is not part of the total porosity of the rock, even though it affects the response of the neutron log.

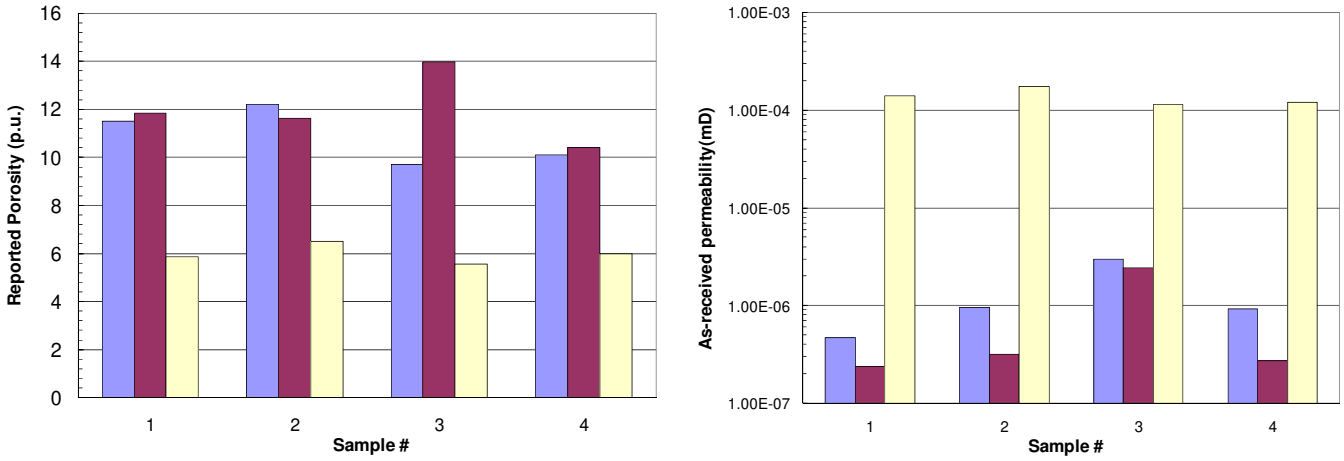

Figure 24 – a) Comparison of "crushed rock" porosity values from three different commercial laboratories.
b) As-received permeability values reported by the same commercial laboratories on splits from the same samples.

Quantification of Permeability (comparison of various labs)

Absolute permeability (referred to as permeability hereafter) of conventional rocks is measured on plug samples under reservoir stress using various methods such as the steady state approach or pulse decay methods. Some of these methods have been used with reasonable success on low permeability rocks (Hsieh et. al., 1981; Yang and Aplin, 2009). For shale-gas reservoirs, the method commonly used is similar to that published by the Gas Research Institute (Luffel et al., 1993; Guidry et. al., 1996), where permeability of the rock matrix is measured using a pressure decay on crushed rock samples. Just as in case of porosity measurements, the permeability values measured on crushed rocks in the absence of reservoir stress can be quite different from the in-situ matrix permeability values. As in case of porosity measurements, we conducted a comparative study of matrix permeability measured by different laboratories using the pressure decay approach on crushed rock samples, where each laboratory received preserved sample splits of rock from the same depth intervals. The results are shown in Figure 24b. The permeability values reported by different laboratories vary by 2-3 orders of magnitude (see also Sondergeld et al., 2010b). The reported values are as-received permeability and one of the sources of observed discrepancies may be differences in sample handling as discussed earlier. One of the primary difficulties in discerning the source of inter-laboratory variation in permeability values is due to the absence of published mathematical formulations used in interpretation of the pressure decay response. Service laboratories have developed their own formulation to analyze results that they hold proprietary, and it is difficult to conclude if the differences in reported values are due to the differences in pressure response data or the interpretation of the results. The observed differences in the laboratory shale-gas rock property measurements suggest that development of industry-wide standard and robust procedures for these measurements are necessary so that the results can be used with greater confidence.

Distribution and Morphology of Pores

High-resolution scanning-electron microscopy of ion-beam milled samples has yielded insight into the occurrence of yet another porosity system contained mainly within the organic matter (Klimentidis et al., 2010; Loucks et al, 2009; Ambrose et al., 2010; Sondergeld et al., 2010). In some overmature organic-rich rocks, it appears that as much as 50% of the volume of the original organic matter may consist of these pores. Thus, the pore volume within the organic matter may be a substantial fraction of the entire porosity of some shale-gas systems (Figure 25). The genesis of these organic-matter pores may represent a phenomenon such as “coking”, observed in retorting of coals. It appears that these pores are contained mainly within the organic matter, and therefore may have entirely different wetability than that of the pores in the mineral matrix. The organic pores may be hydrocarbon wet and could be where the majority of the free gas resides in these overmature organic-rich shale-gas reservoirs. A full understanding of the relation of the porosity and gas should result in development of optimized processes for hydrocarbon recovery in shale-gas reservoirs.

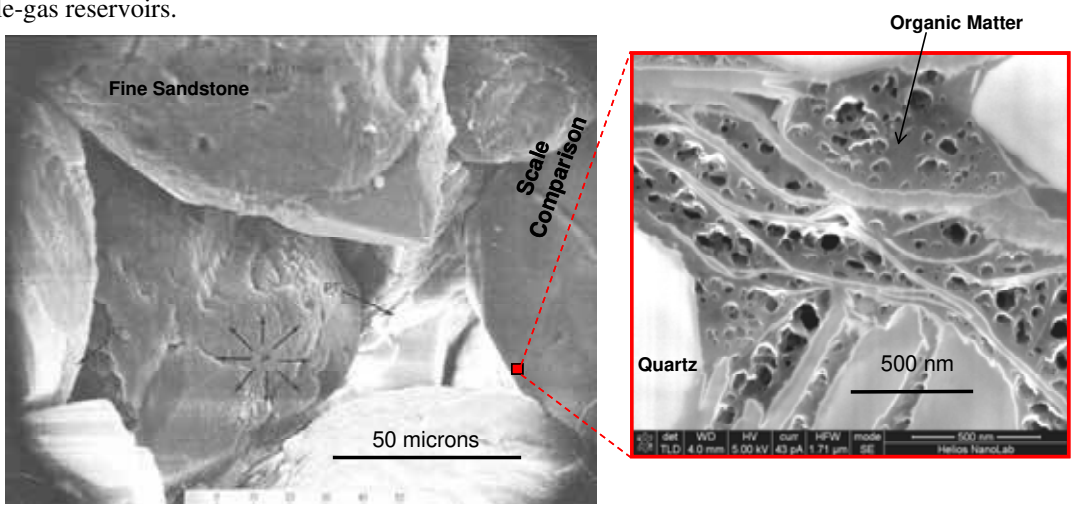

Figure 25 – a) SEM photomicrograph of a fine-grained sandstone and b) comparison of scale of porosity observed in organic matter in a Barnett organic-rich rock. The scale bar for the sandstone is 50 microns and 500 nm for the organic matter inset image, representing two orders of magnitude difference in scale.

Previously, it was discussed how TOC in wt% corresponds to about double that in terms of vol%, due to the lower grain density of the organic matter (e.g., 1.1-1.4 g/cc, compared to 2.6-2.8 g/cc for common rock minerals). The occurrence of pores within the organic matter further amplifies how of a relatively small amount of TOC (in wt%) can impact a much larger volume %, as shown in Figure 26. If 50% of the original organic matter volume is now pores, the volume impacted by the current 5 wt% TOC is

approximately 20 vol% of the rock; thus, the current 5 wt% TOC may impact a volume up to four times its current wt%. Because well logs respond primarily to volume percent of the rock, it is important to understand the difference between current TOC wt% and original TOC vol%.

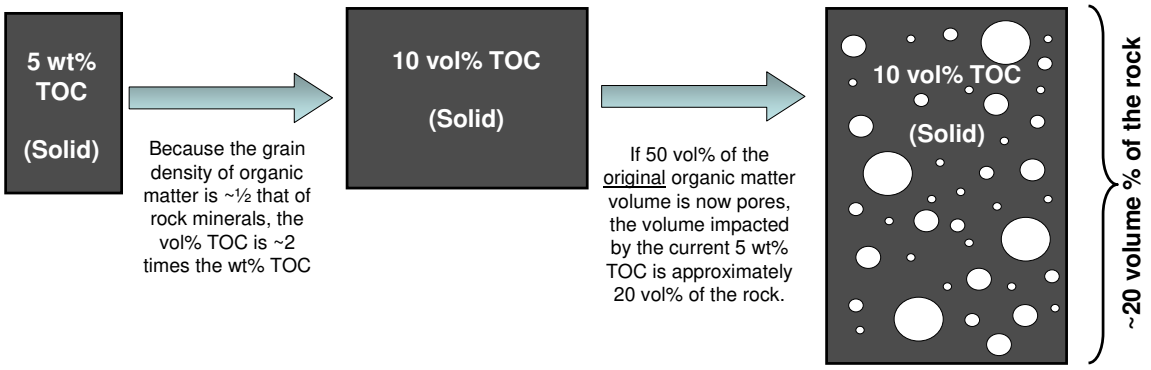

Figure 26 – Schematic illustrating how current 5 wt% TOC corresponds to current10 vol% TOC, but if much of the volume of the original organic matter volume is now occupied by pores within the organic matter, then the current 5 wt% TOC impacts a volume up to 20 vol% of the current rock.

Although a significant portion of the total porosity may be contained in the organic matter, in many formations, porosity within the rock matrix (e.g., intergranualar porosity) can be significant (e.g., clay-rich mudstones and/or mudstones that may have undergone complex diagenetic processes). Due to the very small size of pores in mudstones (and in the associated organic matter), quantification of porosity types in mudstones remains a challenge.

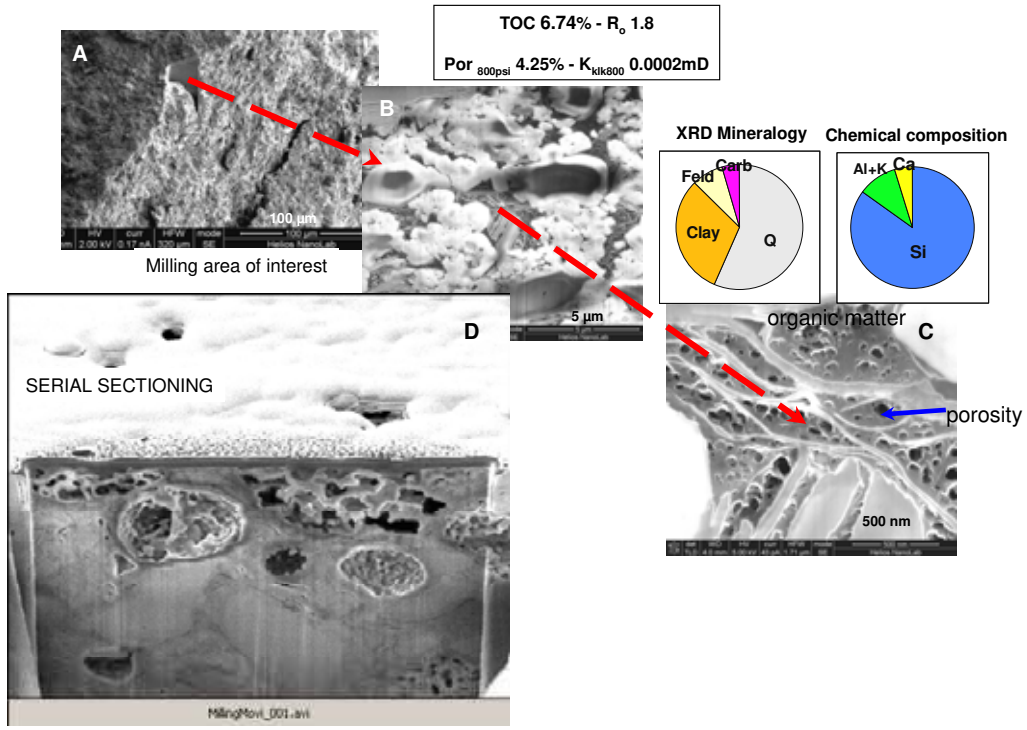

Figure 27 – Successive SEM images using ion-milling to generate serial sections that can be reconstructed as a 3D representation of nanoscale features. Overall, this sample is composed of > 50 wt% quartz, 30wt% clay, and the rest being feldspar and carbonate; this sample contained 6.8 wt% TOC at vitrinite reflectance of 1.8 (LOM 13).

The process of ion-milling successive planes in a SEM/FIB to generate a 3D volume is illustrated in Figure 27. An area of interest is selected in the sample, and examination of this interval is shown at various magnifications (A-C); note that the area of interest represents a very small portion of the rock sample, but provides a unique 3D representation of the distribution and sizes of the

organic matter, mineral matrix, and porosity within each component. Successive slices are milled (Fig 27-D), commonly using a focused-Ga ion beam, and the serial images (slices) are then aligned and corrected for various distortions due to sample position and image artifacts to produce an accurate 3D volume (Figure 28). For this sample, the porosity and permeability values reported are from helium porosimetry on a core plug at confining pressure, and the values may not agree with measurements using crushed-rock methods.

The 3D cube (Figure 28a) allows for investigation of the distribution of organic matter (green phase) and porosity within the organic matter (yellow). Further analysis of this sample yielded a detailed view of the complex connective network of these pores (Figure 28b). The data in the 3D cube can be further analyzed to quantify porosity, pore size distribution, pore connectivity, absolute permeability, relative permeability and elastic properties.

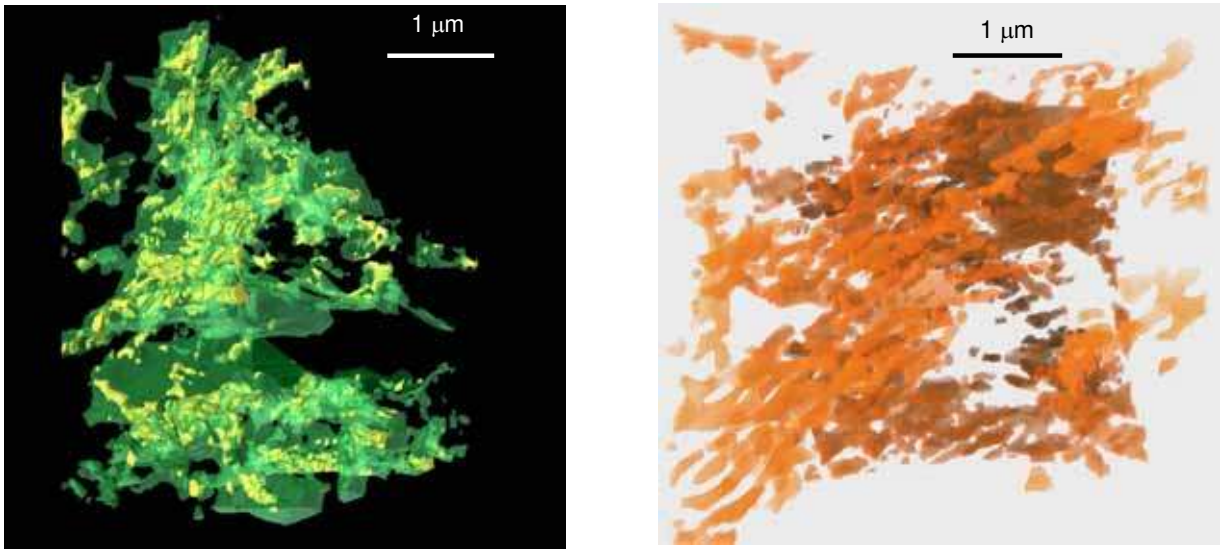

Figure 28 – a) 3D visualization of the organic network (green) and porosity (yellow) (courtesy FEI Company).
b) Image of the connected pore network from the sample shown in (a) (courtesy Mark Knackstedt and Trondt Varslot, ANU). Note the planar alignment of the pore network in this particular 3D view.

Fluid Saturation Determination

Bulk Volume Gas Versus Gas Saturation: Due to significant differences among various commercial labs in evaluating porosity in mudstones (as previously discussed), the use of a gas saturation (Sg) term is problematic and can be misleading. For example, if a rock contains 4% bulk volume gas (BVG) is sent to three laboratories, each measuring a different "porosity", the resulting fluid saturations could greatly vary (e.g., Sg=25% to Sg=80%; Figure 29). This extreme case illustrates the practical problem encountered by users of reported "porosity" and "saturation" data obtained from different laboratories. The bulk volume gas (BVG) measurement from all laboratories, however, should be consistent, so for shale-gas reservoirs the focus should be more on accurate bulk volume gas determination, and less on porosity and conventional gas and water fluid saturations (Sg and Sw).

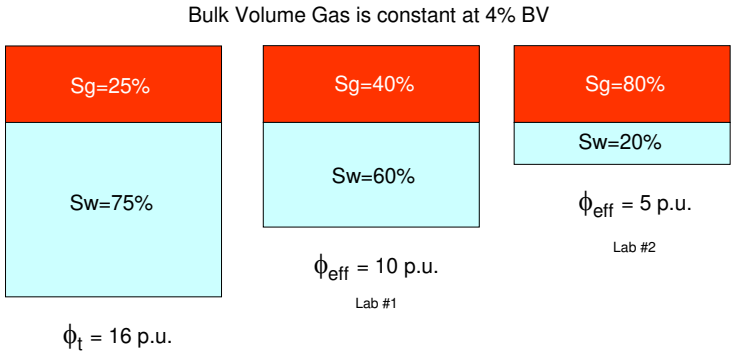

Figure 29 – Schematic showing how a fixed bulk volume of gas (4% BVG), can result in a huge range in fluid saturation numbers depending on what value was used as the reference porosity (which may be depend on the specific laboratory technique or commercial laboratory used for the analyses).

Our observations are that most commercial labs are measuring physical properties of the shale-gas formations (albeit slightly different properties from each other), and that each laboratory's results can be used for calibration of well logs; problems arise when mixing results from one laboratory with those from another laboratory on a given shale-gas formation, or when different assets are compared and different laboratories were used for each asset.

Finally, the insight that small (<100 nm) pores occur in highly overmature oil-prone organic matter allows for speculation about where the gas and water reside in shale-gas formations. Figure 30 represents a conjecture that the pores within the organic matter are filled with gas (both free gas and adsorbed gas on the surface of hydrocarbon-wet organic pores, shown in red). Much of the water in the system is likely to be adsorbed on and associated with the surface of clay minerals (as indicated by the blue lines). Thus, it is likely that gas occupies and is produced from a pore system largely independent from the intergranular water-wet matrix pore system. Given that the pores within the organic matter appear to be interconnected (Figure 28b), this may help explain why shale-gas systems can be so productive. The ultimate key for successful exploitation is in the understanding of how hydraulic fractures intersect and connect with this gas-filled porosity.

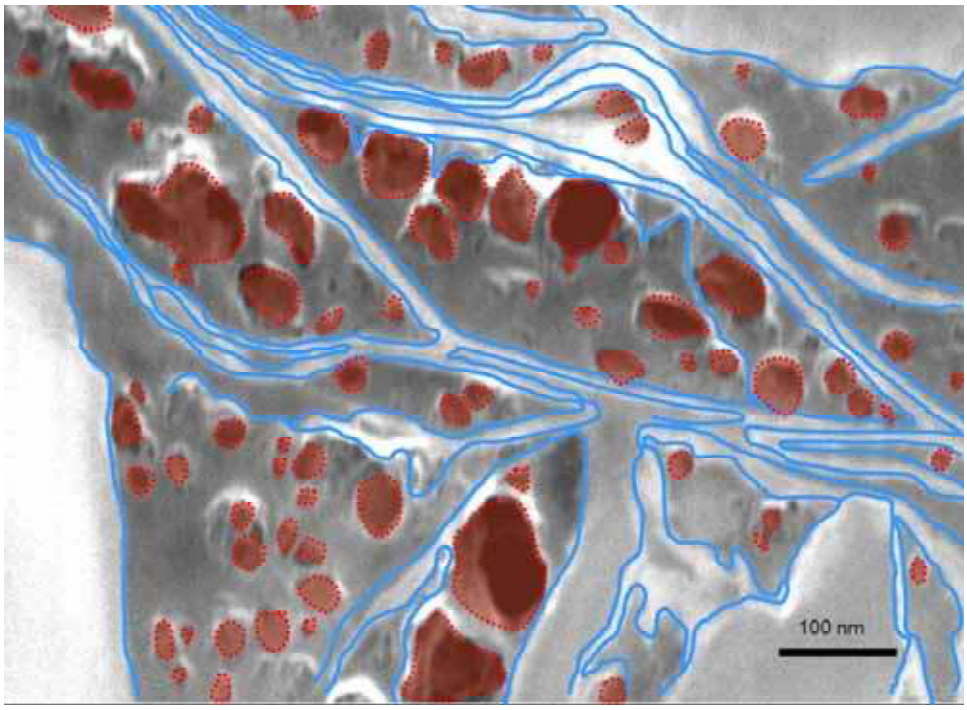

Figure 30 – Hypothetical distribution of gas (red) and water (blue) in organic matter (gray) in this image of an ion-milled Barnett Shale sample. Note that adsorbed gas likely resides on the pore wall (as shown by the small red dots lining each pore). The nominal size of a methane molecule is 0.37 nm, so each small red dot is about 10 times actual size.

Summary and Conclusions

The occurrence and distribution (vertical and lateral) of organic matter in mudstones is well understood using geologic and biotic controls. The vertical distribution of organic matter is a function of production, destruction, and dilution. The basic building block of packages of TOC is the parasequence. In proximal locations, where dilution by clastic sedimentation plays a primary role, the resulting vertical distribution of TOC is the often observed "high TOC at the base, decreasing upward" profile. In distal locations where clastic input in minimal and primary production dominates, TOC can increase upward.

The vertical distribution of TOC can be discerned using a variety of well logs. Methods developed for evaluating immature and mature oil-prone source rocks are readily applied to "overmature" shale-gas formations; these shale-gas rocks are essentially just highly overmature oil-prone source rocks. Modification of the calibration to apply the ΔlogR well log approach for predicting TOC prediction is required for accurate TOC calculation for shale-gas reservoirs of high maturity (Ro>1.0).

Large variability in matrix lithologies is observed when comparing shale-gas plays worldwide. Moreover, large ranges in lithology are observed within a single shale-gas formation and at a vertical scale of a few to 10s of centimeters. A single lithologic or mineralogic property is insufficient to adequately characterize any single shale-gas system.

Porosity and permeability determinations of mudstones are challenging due to the very small particles and pores within the matrix, and this is compounded by the occurrence of connected pores within the organic matter, which may be hydrocarbon wet. The variability of approaches and results in measuring porosity is troublesome in that porosity is often viewed as "the fundamental ground truth" from which all other measurements are based. In clay-rich mudstones, the fundamental definition of porosity is complicated by the high surface area of clay minerals (external and sometimes internal), the volume of surface water (adsorbed first layer, plus the double layer), and the presence of water held by capillary forces in very small matrix pores. We think that much of the variability observed in porosity measurements between commercial service companies results from different definitions of "porosity". Because of the problems in defining porosity, we recommend that saturation terms (e.g., Sw, Sg) that relate to porosity not be used routinely in evaluation of shale-gas reservoirs, but that the focus be on bulk volume gas (BVG), also often referred to as gas-filled porosity. BVG should be consistent between various laboratories, if measured on samples that have not been allowed to dry (i.e., preserved samples). For dry rock samples, measurements of total porosity are recommended for comparison with the logs.

Acknowledgements

We thank ExxonMobil and partners for permission to publish this paper. We thank many individuals for discussions regarding the topics and results in this paper including Andrew Foulds, Dave Dudus, Dale Fitz, Russell Spears and Nabanita Gupta for relevant petrophysical concepts, and Remus Lazar, Tim Demko, Jay Kalbas, Rene Jonk, Jeff Ottmann, Joe Macquaker, and Jurgen Schieber, for exciting and passionate discussions of "mud". FEI Company graciously provided the 3D representation of the ion-milled Barnett sample, and Mark Knackstedt and Trondt Varslot at Australia National University provided the image of the organic pore-connectivity for this same sample. Mark Rudnicki graciously provided a technical review of an earlier draft which greatly improved the readability of the paper. Finally, we thank Mark Lappin, Mike Smith, Ian Russell, Ganesh Dasari, Stefan Boettcher, Pete Rumelhart and Loren Regier for ongoing management support for this research and this paper.

Nomenclature

BI	Bioturbation index
BVG	Bulk volume gas (often referred to as gas-filled porosity)
BVW	Bulk volume water
D	Grain size
g	Acceleration of gravity
HI	Hydrogen index (hydrogen: carbon ratio)
K	Carrying capacity of environment
i	Oxidant species (O_2, SO, etc.)
I	Light intensity
LOM	Level of Organic Metamorphism - a measure of thermal maturity
m	Specific loss rate of phytoplankton
N	Nutrient availability
N_0	Initial number of individual phytoplankton cells
O	Oxidant concentration
$\hat{O}$	In situ oxidant consumption
OI	Oxygen index (oxygen: carbon ratio)
ORR	Organic-rich rock
P	Phytoplankton population density (cells/m3)
q_s	Sediment flux
r	Intrinsic growth rate of population
Ro	Vitrinite reflectance - a measure of thermal maturity
t	Time
TOC	Total organic carbon measured in weight percent (wt%)
SEM	Scanning Electron Microscopy
Sg	Gas saturation (% of pore volume)
Sw	Water saturation (% of pore volume)
x, y, z	Cartesian directions
η	Diffusion gradient of oxidant species
κ	Vertical turbulent diffusivity
μ	Specific growth rates of phytoplankton

ν Phytoplankton sinking velocity
ρ Fluid density
ρ_s Sediment density
τ Bottom shear stress
τ_c Critical bottom shear stress for initiation of motion
ϕ_t Total porosity (total of void space in a rock not occupied by crystalline minerals or organic matter; excludes hydroxyls)
ϕ_{eff} Effective porosity (generally considered as $\phi_{eff} = \phi_t$ - surface bound water)

References

1. Ambrose, R. J., Hartman, R. C., Diaz-Campos, M., Akkutla, I. Y, and Sondergeld, C. H., 2010, New Pore-Scale Considerations for Shale Gas in Place Calculations, SPE-131772, SPE Unconventional Gas Conference, Pittsburgh, Pennsylvania, 23-25, February 2010.
2. Anderson, B., Barber, T., Luling, M., Sen . P., Taherian, and Klein, J., 2008, Indentifying Potential Gas-Producing Shales from Large Dielectric Permittivities Measured by Induction Quadrature Signals, SPWLA Symposium, Edinburgh, Scotland, 25-28 May, 2008, Paper HHHH.
3. Arthur, M.A., Schlanger, S.O., and Jenkyns, H.C., 1987, The Cenomanian–Turonian Oceanic Anoxic Event, II. Palaeoceanographic Controls on Organic Matter Production and Preservation, in Brooks, J., and Fleet, A., eds., Marine Petroleum Source Rocks: Geological Society of London, Special Publication 26, p. 401–420
4. Archie, G. E., 1942, The Electrical Resistivity Log as an Aid in Determining Some Reservoir Characteristics, Trans. Am. Inst. Mining, Metallurgical, and Petroleum Eng. 146, p. 54-62.
5. Berger, W.H., 1976, Biogenous Deep Sea Sediments: Production, Preservation and Interpretation, in Riley, J.P., and Chester, R., eds., Chemical Oceanography: New York, Academic Press, 5, p. 265-388.
6. Bessereau, G., and Guillocheau, F., 1995, Stratigraphie Séquentielle et Distribution de la Matière Organique dans le Lias du bassin de Paris: Académie des Sciences (Paris), Comptes Rendu, 316, p. 1271–1278
7. Bhuyan, K., and Passey, Q. R., 1994, Clay Estimation from GR and Neutron-Density Porosity Logs," SPWLA 35th Annual Logging Symposium, June 19-22, 1994, Paper DDD.
8. Bogdanov, Y.A., Gurvich, Y.G., and Lisitzin, A.P., 1980a, Model for the Accumulation of Calcium Carbonate in Bottom Sediments of the Pacific Ocean: Geochemistry International, 17, p. 125–132.
9. Bogdanov, Y.A., Gurvich, Y.G., and Lisitzin, A.P., 1980b, A Model for the Accumulation of Amorphous Silica in Pacific Sediment: Geochemistry International, 17, p. 51–56.
10. Bohacs, K.M., 1990, Sequence Stratigraphy of the Monterey Formation, Santa Barbara County: Integration of Physical, Chemical, and Biofacies Data from Outcrop and Subsurface: SEPM, Core Workshop 14, San Francisco, Ca.
11. Bohacs, K.M., 1993, Source Quality Variations Tied to Sequence Development in the Monterey and Associated Formations, Southwestern California, in Katz, B.J., and Pratt, L.M., eds., Petroleum Source Rocks in a Sequence-Stratigraphic Framework: AAPG Studies in Geology, 7, p. 177–204.
12. Bohacs, K.M., 1998, Contrasting Expressions of Depositional Sequences in Mudstones from Marine to Non-marine Environs, in Schieber, J., Zimmerle, W., and Sethi, P., eds., Mudstones and Shales, vol. 1, Characteristics at the Basin Scale: Stuttgart, Schweizerbart'sche Verlagsbuchhandlung, p. 32–77.
13. Bohacs, K. M., and Lazar, O. R., 2010, Sequence Stratigraphy in Fine-Grained Rocks at the Field to Flow-unit Scale: Insights for Correlation, Mapping, and Genetic Controls, presented at Houston Geological Society, Applied Geoscience Conference, February 8-9, 2010, Houston.
14. Bohacs, K.M., Miskell-Gerhardt, K., 1998, Well-log expression of lake strata; controls of lake-basin type and provenance, contrasts with marine strata. AAPG Annual Meeting Expanded Abstracts, Tulsa, Oklahoma, p. A78.
15. Bohacs, K. M., Grawbowski, G. J., Carroll, A. R., Mankeiwitz, P. J., Miskell-Gerhardt, K. J., Schwalbach, J. R., Wegner, M. B., and Simo, J. A, 2005, Production, Destruction, and Dilution – the Many Paths to Source-Rock Development, SEPM Special Publication 82, p. 61-101.
16. Boles, J.R. and Franks, S.G., 1979, Clay Diagenesis in Wilcox Sandstones of Southwest Texas; Implications of Smectite Diagenesis on Sandstone Cementation, Journal of Sedimentary Petrology, 49, p. 55-70.
17. Brumsack, H. J., 1980, Geochemistry of Cretaceous Black Shales from the Atlantic Ocean (DSDP Legs 11, 14, 36, and

41): Chemical Geology, 31, p. 1–25.

18. Bustin, R. M., Bustin, A. M., Cui, X., Ross, D.J.K., Murthy, Pathi, V. S., 2008, Impact of Shale Properties on Pore Structure and Storage Characteristics, SPE-119892, SPE Shale Gas Production Conference, Fort Worth, Texas, 16-18 November, 2008.
19. Creaney, S., and Passey, Q. R., 1993, Recurring Patterns of Total Organic Carbon and Source Rock Quality within a Sequence Stratigraphic Framework, AAPG Bulletin 77, p. 386-401.
20. Eslinger, E. and Pevear, D., 1988, Clay Minerals for Petroleum Geologists and Engineers, SEPM Short Course 22.
21. Feibelman, P., 2010, The First Wetting Layer on a Solid, Physics Today, February 2010, p.34-39.
22. Grossart, H. P., Simon, M., and Logan, B. E., 1997. Formation of Macroscopic Organic Aggregates (Lake Snow) in a Large Lake: The Significance of Transparent Exopolymer Particles, Phytoplankton and Zooplankton. Limnol. Oceanogr. 42, p. 1651–1659.
23. Grabowski, G.J., and Glaser, K.S., 1990, Depositional Model for Transgressive Marine Organic-rich Rocks Formed in Platform Settings: Middle Callovian and Lower Toarcian Examples from Onshore England. 13th International Sedimentological Congress, Nottingham, 196 pp.
24. Guidry, F.K., Luffel, D.L, Curtis, J.B., 1996, Development of Laboratory and Petrophysical Techniques for Evaluating Shale Reservoirs, Gas Research Institute, GRI - 5/0496.
25. Guthrie, J.M., and Bohacs, K.M., 2009, Spatial Variability of Source Rocks: a Critical Element for Defining the Petroleum System of Pennsylvanian Carbonate Reservoirs of the Paradox Basin, SE Utah. *in* W.S. Houston, L.L. Wray, and P.G.Moreland, eds., The Paradox Basin Revisited -- New Developments in Petroleum Systems and Basin Analysis, RMAG 2009 Special Publication -- the Paradox Basin, p. 95-130.
26. Hartnett, H.E., Keil, R.G., and Hedges, J.I., 1998, Influence of Oxygen Exposure Time on Organic Carbon Preservation in Continental Margin Sediments: Nature, 391, p. 572–574.
27. Heinrichs, S.M., and Reeburgh, W.S., 1987, Anaerobic Mineralization of Marine Sediment Organic Matter: Rates and the Role of Anaerobic Processes in the Oceanic Carbon Economy: Geomicrobiology Journal, 5, p. 191–238.
28. Heckel, P.H., 1972, Recognition of Ancient Shallow Marine Environments, in Rigby, J.K., and Hamblin, W.K., eds., Recognition of Ancient Sedimentary Environments: SEPM Special Publication 16, p. 226–286.
29. Hood, A., Gutjahr, C. M., and Heacock, R. L., 1975, Organic Metamorphism and the Generation of Petroleum, AAPG Bulletin, 59, p. 986-996.
30. Hsieh, P.A., Tracy, J.V., Neuzil, C.E., Bredehoeft, J.D., Silliman, S.E., 1981, A Transient Laboratory Method for Determining the Hydraulic Properties of 'Tight' Rocks - I. Theory., Int. J. Rock Mech.Min. Sci. Geomech. Abstr. 18, p. 245-252.
31. Huc, A.Y., 1988, Aspects of Depositional Processes of Organic Matter in Sedimentary Basins: Organic Geochemistry, 13, p. 263–272.
32. Huc, A.Y, 1995, Paleogeography, Paleoclimate, and Source Rocks, AAPG Studies in Geology 40, 347 p.
33. Isaacs, C.M., 1987, Sources and Deposition of Organic Matter in the Monterey Formation, South-central Coastal Basins of California, in Meyer, R.F., ed., Exploration for Heavy Crude Oil and Natural Bitumen: AAPG Studies in Geology, 25, p. 193–205.
34. Jacobi, D., Breig, J., LeCompte, B., Kopal, M., Hursan, G., Mendez, F., Bliven, S., and Longo, J., 2009, Effective Geochemical and Geomechanical Characterization of Shale Gas Reservoirs from the Wellbore Environment: Caney and Woodford Shale, SPE 123231, SPE Annual Tech. Conference, New Orleans, Louisiana, USA, 4-7 October 2009.
35. Jarvie, D.M., Hill. R. J., Ruble, T. E., and Pollastro, R.M., 2007, Unconventional Shale-gas Systems: The Mississippian Barnett Shale of North-central Texas as One Model for Thermogenic Shale-gas Assessment, AAPG Bull. 91, p. 475-499.
36. Katz, B.J., and Pratt, L.M., eds., 1993, Petroleum Source Rocks in a Sequence-Stratigraphic Framework: AAPG Studies in Geology, 7, 247 pp.
37. Klimentidis, R., Lazar, O. R., Bohacs, K. M, Esch, W. L., and Pedersen, P., 2010, Integrated Petrography of Mudstones, AAPG 2010 Annual Convention, New Orleans, Louisiana, April 11-14.
38. Leckie, D. A., Singh, C., Goodarzi, F., and Wall, J. H., 1990, Organic-rich Radioactive Marine Shale: a Case Study of a Shallow-water Condensed Section, Cretaceous Shaftsbury Formation, Alberta, Canada, Jour. Sed. Pet. 60, p. 101-117.

39. Logan, B. E., Passow, U., Alldredge, A. L, Grossart, H. P., and Simon, M., 1995. Rapid Formation and Sedimentation of Large Aggregates is Predictable from Coagulation Rates (Half-lives) of Transparent Exopolymer Particles (TEP), Deep-Sea Res. II. 42, p. 203–214.
40. Loucks, R. G., Reed, R. M., Ruppel, S. C., and Jarvie, D. M., 2009, Morphology, Genesis, and Distribution of Nanometer-Scale Pores in Siliceous Mudstones of the Mississippian Barnett Shale, Jour. Sedimentary Research 79, p. 848-861.
41. Luffel, D.L., Guidry, F.K. and Curtis, J. B., 1992, Evaluation of Devonian Shale with New Core and Log Analysis Methods, J. Pet. Tech, Nov.: 1192-1197, SPE21297.
42. Luffel, D.L., and Guidry, F. K., 1992, New Core Analysis Methods for Measuring Reservoir Rock Properties of Devonian Shale, J. Pet. Tech, Nov. 1182-1190, SPE 20571.
43. Luffel, D. L., Hopkins, C W., Holditch, S. A., and Schettler, P. D., 1993, Matrix Permeability Measurement of Gas Productive Shales, SPE 26633, 261-270.
44. Merkel, R. H., and Gegg, J. F., 2008, NMR Log/Core Data in Tight Gas Sand Petrophysical Model Development, SPWLA Annual Symposium, Edinburgh, Scotland, 25-28, 2008, Paper CC.
45. Meyer, B. I., and Nederlof, M. H, 1984, Identification of Source Rocks on Wireline Logs by Density/Resistivity and Sonic Transit Time/Resistivity Cross plots, AAPG Bulletin, 68, p. 121-129.
46. Miskell-Gerhardt, K.J., 1989, Productivity, Preservation, and Cyclic Sedimentation within the Mowry Shale Depositional Sequence, Western Interior Seaway: unpublished Ph.D. dissertation, Rice Univ., Houston, Texas, 432 p
47. Passey, Q., R., Dahlberg, K. E., Sullivan, K. B., Yin, H., Brackett, R. A., Xiao, Y. H., and Guzman-Garcia, A. G., 2006, Petrophysical Evaluation of Hydrocarbon Pore-Thickness in Thinly Bedded Clastic Reservoirs, AAPG Archie Series, No. 1, 210 pp.
48. Passey, Q. R., Creaney, S., Kulla, J. B., Moretti, F. J., and Stroud, J. D., 1990, A Practical Model for Organic Richeness from Porosity and Resistivity Logs, AAPG Bulletin, 74, p. 1777-1794.
49. Passow, U., Alldredge, A. L, and Logan, B. E., 1994. The Role of Particulate Carbohydrate Exudates in the Flocculation of Diatom Blooms. Deep-Sea Res. I. 41, p. 335–357.
50. Potter, P.E., Maynard, J.B., and Pryor, W.A., 1980, Sediment logy of Shale, New York, Springer-Verlag, 310 pp.
51. Ricken, W., 1993, Sedimentation in a Three-component System, Berlin, Springer-Verlag, Lecture Notes in Earth Sciences, 51.
52. Savarda, C.E., and Bottjer, D.J., 1986, Trace-fossil Model for Reconstruction of Paleo-oxygenation in Bottom Waters: Geology, 14, p. 3–6.
53. Savarda, C.E., and Bottjer, D.J., 1991, Oxygen-related Biofacies in Marine Strata: an Overview and Update, in Tyson, R.V., and Pearson, T.H., eds., Modern and Ancient Continental Shelf Anoxia: Geol. Soc. London, Special Publications 58, p. 201–219.
54. Schieber, J., Southard, J.B., and Thaisen, K., 2007, Accretion of Mudstone Beds from Migrating Floccule Ripples, Science, 318, p. 1760-1763.
55. Schwarzkopf, T.A., 1993, Model for Prediction of Organic Carbon in Possible Source Rocks, Marine and Petroleum Geochemistry, 10, p. 478–492.
56. Schwalbach, J.R., Bohacs, K.M., and Gorsline, D.S., 1993, Sediment Accumulation Rates in Distal Marine Settings: Western North American Continental Margins, in Armentrout, J.M., Bloch, R., Olson, H.C., and Perkins, Bob F., eds., Rates of Geological Processes: Tectonics, Sedimentation, Eustacy and Climate, Implications for Hydrocarbon Exploration: SEPM Foundation, Gulf Coast Section, Fourteenth Annual Research Conference, p. 229–233
57. Schwalbach, J.R., and Bohacs, K.M., 1992, Sequence Stratigraphy in Fine-grained Rocks: Examples from the Monterey Formation: SEPM, Pacific Section, Guidebook 70, 80 p.
58. Sondergeld, C. H., Ambrose, R. J., Rai,C. S., and Moncrieff, J., 2010a, Micro-Structural Studies of Gas Shales, SPE 131771, SPE Unconventional Gas Conference, Pittsburgh, Pennsylvania, 23-25 February, 2010.
59. Sondergeld, C. H., Newsham, K. E., Comisky, J. T., Rice, M. C., and Rai, C. S., 2010b, Petrophysical Considerations in Evaluating and Producing Shale Gas Resources, SPE 131768, SPE Unconventional Gas Conference, Pittsburgh, Pennsylvania 23-25, 2010.

60. Spears, R., W., and Jackson, S.,L., 2009, Development of a Predictive Tool for Estimating Well Performance in Horizontal Shale Gas Wells in the Barnett Shale, North Texas, USA, Petrophysics, 50, p. 19-31.

61. Strakhov, N.M., 1971, Geochemical Evolution of the Black Sea in the Holocene: Lithology and Mineral Resources, 6, p. 263–274.

62. Summerhayes, C.P., and Masran, T.H., 1983, Organic Facies of Cretaceous and Jurassic Sediments form DSDP Site 534 in the Blake Bahama Basin, Western North America, in Sheridan, R.E., Gradstein, F., et al., eds., Initial Reports of the Deep Sea Drilling Program: Washington, D.C., U.S. Government Printing Office, 76, p. 469–480 .

63. Tada, R., 1991, Origin of Rhythmical Bedding in Middle Miocene Siliceous Rocks of the Onnagawa Formation, Northern Japan: Jour. Sed. Pet., 61, p. 1123–1145.

64. Thyburg, B., Jahren, J., Winje, T., Bjorlykke, K., and Faleide, J. I., 2009, From Mud to Shale: Rock Stiffening by Micro-quartz Cementation, EAGE First Break, 27, February 2009, p. 53-59.

65. Tissot, B. P., and Welte, D. H., 1984, Petroleum Formation and Occurrence, Springer-Verlag: New York, 699 pp.

66. Tyson, R.V., 1995, Sedimentary Organic Matter; Organic Facies and Palynofacies: London, Chapman & Hall, 615 pp.

67. Tyson, R.V., 2001, Sedimentation Rate, Dilution, Preservation and Total Organic Carbon: Some Results of a Modeling Study, Organic Geochemistry, 32, p. 333–339.

68. Vanney, J. R., and Stanley, D. J., 1983, Shelfbreak Physiography: An Overview, in D. J. Stanley, & G. T. Moore eds., The Shelfbreak: Critical Interface on Continental Margins, SEPM Special Publication 33, p. 1-24.

69. van Rijn, L.C., 1984, Sediment Transport, Part II: Suspended Load Transport. Jour. Hydraulic Engineering, 110, p.1613-1641.

70. Waxman, M. H., and Smits, L. J. M, 1968, Electrical Conductivities in oil-bearing Shaly Sands, SPE Jour. 8, p. 107-122.

71. Werne, J. P., Sageman, B. B., Lyons, T. W., and Hollander, D. J., 2002, An Integrated Assessment of a “Type Euxinic” Deposit – Evidence for Multiple Controls on Black Shale Deposition in the Middle Devonian Oatka Creek Formation, Am. Jour. Science, 302, p. 110-143.

72. Wignall, P.B., 1991, Model for Transgressive Black Shales, Geology 19, p 167-170.

73. Wong, M. and Parker, G., 2006, Reanalysis and Correction of Bed-load Relation of Meyer-Peter and Mueller using Their Own Database. Jour. Hydraulic Engineering, 132, p.1159-1168.

74. Worthington, P. F., 1985, Evolution of Shaly Sand Concepts in Reservoir Evaluation, The Log Analyst, 26, p. 23-40.

75. Yang, Y., and Aplin, A.C, 2009, A Permeability-porosity Relationship for Mudstones, Marine and Petr. Geo., p 1-6.

76. Zhu, Y., Martinez, A., Liu, E., Harris, C., Xu, S., Payne, M. A., and Terrell, M., 2010, Understanding Geophysical Responses of Shale Gas Plays, EAGE Shale Workshop, Nice, France, 27 April, 2010.